

Recent advances on fluorescent biomarkers of near-infrared quantum dots for *in vitro* and *in vivo* imaging

Shanmugavel Chinnathambi ^a and Naoto Shirahata ^{b,c,d}

^aInternational Center for Young Scientists, National Institute for Materials Science (NIMS), Tsukuba, Japan;

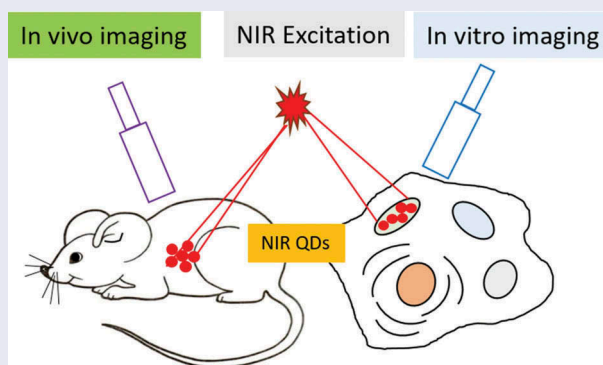
^bInternational Center for Materials Nanoarchitectonics, NIMS, Tsukuba, Japan;

^cGraduate School of Chemical Sciences and Engineering, Hokkaido University, Sapporo, Japan;

^dDepartment of Physics, Chuo University, Tokyo, Japan

ABSTRACT

Luminescence probe has been broadly used for bio-imaging applications. Among them, near-infrared (NIR) quantum dots (QDs) are more attractive due to minimal tissue absorbance and larger penetration depth. Above said reasons allowed whole animal imaging without slice scan or dissection. This review describes *in vitro* and *in vivo* imaging of NIR QDs in the regions of 650–900 nm (NIR-I) and 1000–1450 nm (NIR-II). Also, we summarize the recent progress in bio-imaging and discuss the future trends of NIR QDs including group II-VI, IV-VI, I-VI, I-III-VI, III-V, and IV semiconductors.



ARTICLE HISTORY

Received 12 October 2018

Revised 2 March 2019

Accepted 2 March 2019

KEYWORDS

Quantum dots; bio-marker; NIR imaging; review


CLASSIFICATION

60 New topics / Others: Nanocrystals, Quantum dots, Bioimaging, Biomarkers, Fluorescence imaging; 204 Optics / Optical applications

1. Introduction

Fluorescence imaging is a useful technique for biological applications. Recently, quantum dots (QDs) have become a popular imaging agent, competing with other fluorescent nanomaterials and dyes [1–7]. One more advantage is we can get multiplex emission with single light source excitation with minimal spectral overlap. The outstanding optoelectronic properties of QDs include high quantum yield (QY), size-dependent, and narrow light emission, broad absorption spectrum, massive stoke shift and resistance to photobleaching [8]. In the blood protein and other bio-molecule, sizes are comparable with most available QDs. QDs are prepared in organic or aqueous solutions depending on the proposed applications. Recently, exciting research activities going on in the above said reasons and quality of the materials. Biological imaging started using QDs from 1998, from that moment QD-based bio-imaging and bio-sensing applications developed rapidly [9–13].

For bio-medical applications, it is better to use near-infrared (NIR) region due to low absorption (see Figure 1(a,b)) and autofluorescence from the tissues [14]. Human tissues are made up of several organic molecules that naturally absorb (DNA, collagen, elastin, proteins, NADH, and FAD) and emit (NADH, FAD, proteins and DNA) the light in the ultraviolet to visible region [9]. The NIR emitting QDs for *in vivo* deep-tissue imaging are desirable owing to the improved tissue penetration of lights and decreased tissue autofluorescence in the NIR range of 750–940 nm and 1200–1700 nm. Hence, researchers are developing fluorescent materials with both the excitation and emission wavelengths confined within the biological transparency window (NIR-I: $\lambda_{em} = 750\text{--}900\text{ nm}$) [15]. NIR-I window reduces the scattering and absorbance (due to H₂O, boric acid, metabolic acid, fat, bilirubin, melanosome) of the light and resulting deep penetration in biological tissues. Therefore, it is important to select the optical

CONTACT Naoto Shirahata  SHIRAHATA.Naoto@nims.go.jp  International Center for Materials Nanoarchitectonics, NIMS, 1-1 Namiki, Tsukuba, Japan

© 2019 The Author(s). Published by National Institute for Materials Science in partnership with Taylor & Francis Group.

This is an Open Access article distributed under the terms of the Creative Commons Attribution License (<http://creativecommons.org/licenses/by/4.0/>), which permits unrestricted use, distribution, and reproduction in any medium, provided the original work is properly cited.

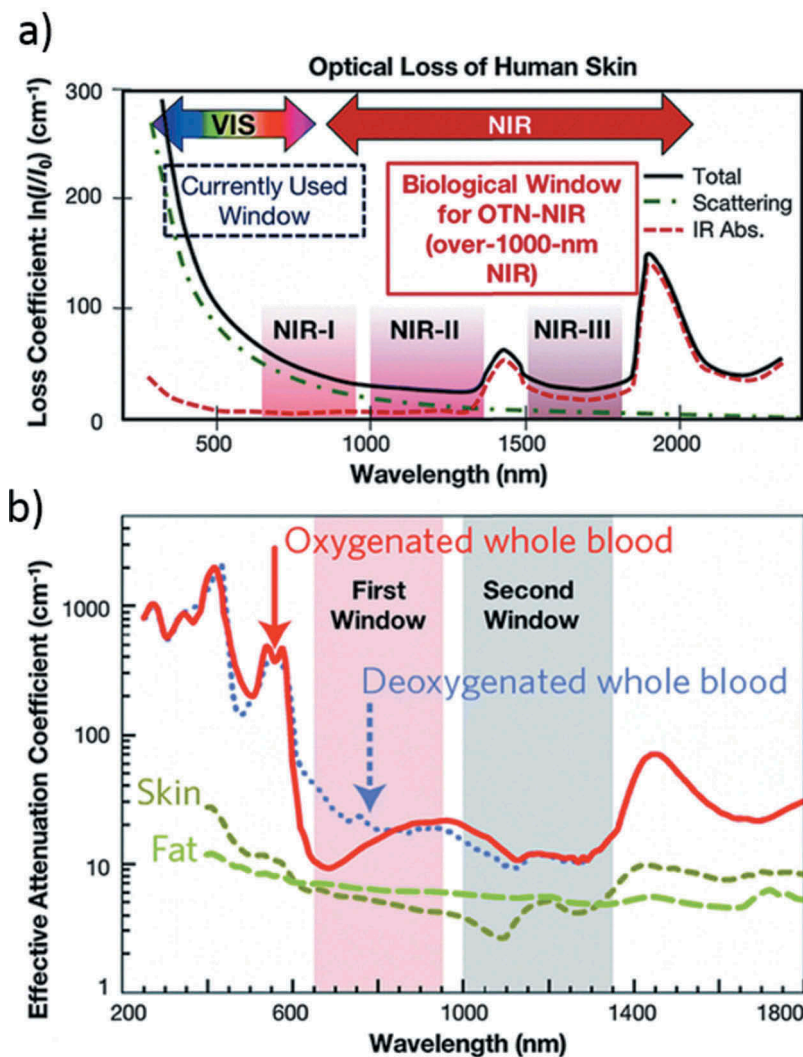


Figure 1. (a) Human skin absorption spectra in the of NIR-I, NIR-II, and NIR-III regions. (b) Absorption and scattering spectra from oxygenated blood, deoxygenated blood, skin and fatty tissue. Reproduced with permission from (Figure 1(a), [14] Copyright 2009 RSC Publishing; Figure 1(b), [18] Copyright 2016 RSC Publishing).

transmission window of the skin (750–940 nm) for NIR imaging. NIR-II window ($\lambda_{em} = 1000\text{--}1700$ nm) was developed for imaging with a tissue penetration depth of more than 2 cm.

Most importantly, QDs must be dispersed in water for biological applications. QDs are synthesized initially in organic nonpolar solvents then surface modification essential to soluble in water. For bio-imaging, bio-sensing, researchers developed NIR QDs with various surface functionalization to get the water-soluble materials [16–19]. The large QDs surface area gives better attachment of the bio-molecules compared with other organic dyes and other bio-molecules. The conventional methods to prepare the water-dispersible QDs are ligand exchange and surface modification with some hydrophilic molecules [20]. Most importantly, QDs are more stable than organic dyes upon light exposure. The main content of this review is QDs which can be emitted in NIR-I and NIR-II regions. Here, mainly we presented the properties of NIR-emitting QDs for bio-imaging applications. Table 1

shows the types of NIR QDs, surface modifications, PL properties, and biological applications. We systematically summarize the recent progress of bio-medical imaging and discuss the shortcomings, challenges, and opportunities in it.

2. Quantum dots for biological imaging

2.1. Group II-VI quantum dots

CdTe and HgTe QDs are most widely used in the NIR region. Gao et al. developed $\text{CdTe}_x\text{Se}_{1-x}/\text{ZnS}$ alloy nanocrystals to achieve QYs up to 80% with controllable rod-shape and NIR ($\lambda_{em} = 650\text{--}870$ nm) emission (Figure 2 (a)) [21]. He et al. reported a facile one-step microwave synthesis of water-soluble CdTe QDs. The water-soluble NIR CdTe QDs ($\lambda_{em} = 700\text{--}800$ nm) are used first time for *in vivo* tumor targeting and also used for *in vitro* imaging after conjugation with protein molecules (Figure 2(b,d,f)) [22]. Recently, Geiregat et al. demonstrated that mercury telluride (HgTe) QDs exhibit size-

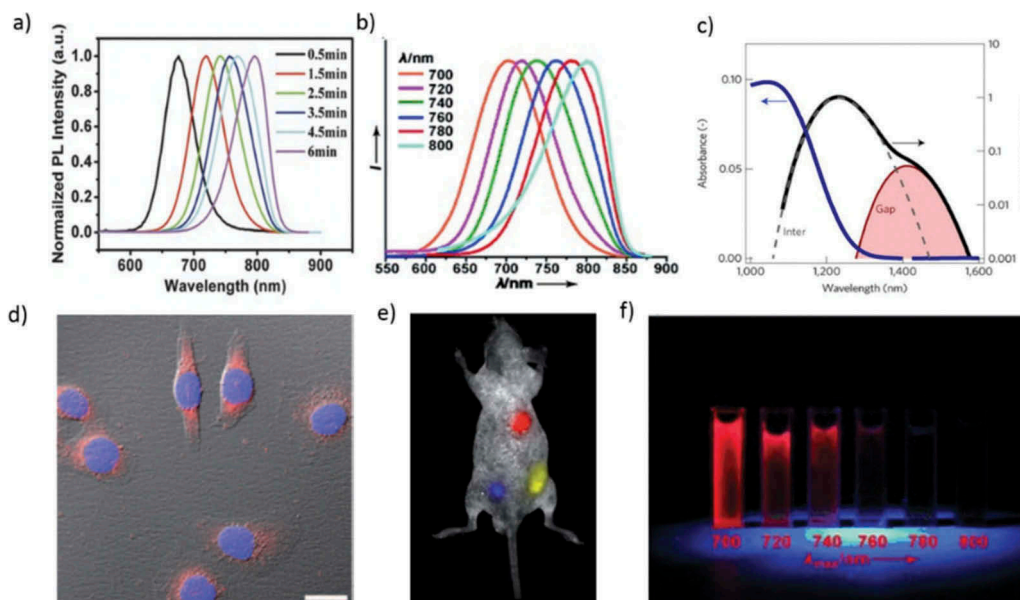


Figure 2. (a) PL emission spectra of CdTe_{0.15}Se_{0.85} QDs under different growth times. (b) NIR QDs with emission tunable from 700–800 nm (excitation = 450 nm). (c) Absorbance (blue) and emission (black) of HgTe QDs suspended in TCE. (d) Dual-color immunofluorescence cellular imaging (scale bar: 20 mm). The HeLa cells are labeled by the QDs/protein conjugates (red) and Hoechst (blue). (e) Multiplex imaging capability of CdTe/CdSe QDs in live animals. (f) CdTe QDs under UV irradiation ($\lambda_{\text{ex}} = 365$ nm). Reproduced with permission from (Figure 2(a), [21] Copyright 2014 Wiley Publishing; Figure 2(b), [22] Copyright 2011 Wiley Publishing; Figure 2(c), [23] Copyright 2018 Nature Publishing Group; Figure 2(d), [22] Copyright 2011 Wiley Publishing; Figure 2(e), [29] Copyright 2011 RSC Publishing; and Figure 2(f), [22] Copyright 2011 Wiley Publishing).

tunable emission all over the NIR window at thresholds unmatched by any QDs studied before (Figure 2(c)) [23]. Alloyed CdTe_{1-x}Se_x/CdS NIR QDs are used for detecting pancreatic cancer in mouse models [24]. Alloyed CdHgTe QDs were prepared via heating a mixture of Cd²⁺, Hg²⁺, and Te²⁻ in the presence of 3-mercaptopropionic acid (MPA) as ligands with photoluminescence (PL) QYs (20–50%) and narrow emission bands and it will be a suitable fluorescent probe in the imaging of living animals [25]. Recently, Liu et al. developed a NIR-emitting CdHgTe/CdS/CdZnS QDs and coated them with three different thiol ligands, 3-MPA, thioglycolic acid (TGA), and N-acetyl-L-cysteine (NAC). *In vivo* toxicity measurement shows negligible harmful effects to nude mice even at a concentration of 20 mg kg⁻¹ [26]. Gadolinium-functionalized CdHgTe/ZnS core/shell QDs are used for *in vivo* fluorescence and magnetic resonance imaging [27]. Cyclic arginine-glycine-aspartic acid conjugated micelle-encapsulated NIR CdTe/ZnSe QDs as highly luminescent probes for bio-labeling and *in vivo* imaging of pancreatic tumor in live mice [28]. In 2011, CdTe/CdSe QDs were also successfully applied for the fluorescence imaging of living animals (Figure 2(e)) [29].

MPA-stabilized NIR-emitting CdTe/CdS QDs have used fluorescence sensor for Cu²⁺ with a low detection limit, and the sensor was applied to the bio-sensing and bio-imaging in the HeLa cells and Kunming mice. The quenching effects resulted from the aggregation of QDs induced by the competitive binding between MPA on the surfaces of the NIR

QDs and the Cu²⁺ present in the solution. The Cu-S bond has a much lower K_{sp} value than that of Cd-S bond. *In vitro* imaging of HeLa cells and *in vivo* imaging of Kunming mice demonstrated that these NIR QDs are suitable for high-resolution imaging of biological tissues owing to the suitable wavelength range of emission light [30].

Lu et al. reported, short-term and long-term *in vivo* bio-distribution, pharmacokinetics, and toxicity of the CdTe QDs. NIR-emitting QDs are initially accumulated in the liver, spleen, and lung for short-time (0.5–4 h) post-injection, and then increasingly absorbed by kidney during long-time (4–94 days) blood circulation. Furthermore, histological and biochemical analyses and body weight measurements demonstrate that there is no overt toxicity of NIR-emitting QDs in mice even during a 94-day exposure [31].

2.2 Group IV-VI quantum dots

Group IV-VI semiconductor QDs are an excellent candidate for biomedical applications due to their unusual electronic and transport properties. QD material purity, surface passivation, reproducible, and high quality were analyzed by a powerful tool like PL characterization. (Figure 3(b)) [32]. Lignos et al. demonstrated a controlled droplet-based microfluidic platform to produce monodisperse PbS and PbSe QDs under a wide range of experimental conditions (Figure 3(a)) [33]. The lowest-energy exciton transitions in PbSe, with diameters

Table 1. Summary of representative QDs and their surface modifications, emission maxima and bio-applications.

Types of QDs	Surface coating	Emission Maximum (nm)	Applications	Ref
II-VI Group				
CdTe	mercaptoundecanoic acid (MPA)	700–800	<i>In vivo</i> tumor targeting	[22]
CdTe/CdSe	PMAS-PEG	801	Multiplex imaging in live animals	[29]
CdTe/ZnSe	phospholipids	730	Imaging of panc-1 tumor-bearing mice	[28]
CdTe _{1-x} Sex/CdS	PEG-grafted phospholipid	845	Cancer imaging and therapy	[24]
CdHgTe/CdS/ZnS	N-acetyl-L-cysteine	650–800	<i>In vivo</i> tumor targeting	[26]
IV-VI Group				
PbS	recombinant protein (GST-EGFP-GB1)	1150	Breast tumor imaging	[44]
PbS	dihydrolipoic acid – polyethylene glycol	1300	Mice <i>in vivo</i>	[45]
PbS	MPA	1100	Imaging of the thrombotic state in septic mouse brain	[35]
PbS	BSA-functionalized AuNCs	813	Bio-imaging of ascorbic acid	[38]
PbS/CdS/ZnS	MPA	1270	<i>In vivo</i> fluorescent imaging agents	[39]
I-VI Group				
Ag ₂ Se	polyethylene glycol (PEG)	1300	Blood Clearance and bio-distribution	[48]
Ag ₂ Se	Multidentate polymer	950–1250	<i>in vivo</i> fluorescence images	[54]
Ag ₂ Se	C ₁₈ -PMH-PEG	1300	<i>In vivo</i> imaging of live mice	[58]
Ag ₂ S	Glutathiose	1015	nitric oxide delivery and fluorescence imaging	[53]
Ag ₂ S	Dihydrolipoic acid	1000–1400	early stage tumor diagnosis	[60]
Ag ₂ S	carboxylic acid group	825	EGFR targeted tumor imaging	[72]
I-III-VI Group				
CuInS ₂	RNase A capped CuInS ₂	700–800	<i>in vivo</i> imaging	[74]
AgInSe ₂ -ZnSe	multidentate polymer	625–940	Cell imaging	[78]
AgInS ₂	multidentate polymer	820	<i>in vivo</i> imaging	[76]
III-V Group				
InAs core-shell	Phospholipid	1280	Multicolor imaging	[84]
	Nanosomes	1300	Quantitative metabolic imaging	
	Composite particles	1280	Blood flow maps	
InAs/InP/ZnSe	MPA	800	Tumor detection in living mice	[85]
IV Group				
Carbon	Ethylenediamine	750	Two-photon fluorescence imaging	[96]
Carbon	S, Se-codoped	731 & 820	fluorescence imaging and photothermal therapy	[95]
Carbon	Poly(vinylpyrrolidone)	750	<i>In vivo</i> NIR fluorescence imaging	[97]
Carbon	PEG-800	600–900	Photothermal Cancer Therapy	[92]
Carbon	Fluorescein isothiocyanate	683	two-photon fluorescence bio-imaging	[93]
Si	Pluronic F127	650	two-photon fluorescence cell imaging	[107]
Si	4,7-di(2-thienyl)-2,1,3-benzothiadiazole	900	Two-Photon Absorbing Antenna	[140]
Si	B,P – codoped	600–1200	time-gated fluorescence imaging in the second near-infrared window	[141]

between 3 and 8 nm, happen at wavelengths between 1.0 and 1.85 μm [34]. Imamura et al. reported PbS QDs and their use for *in vivo* NIR fluorescence imaging of cerebral venous thrombosis in septic mice [35]. PbS QDs were synthesized using an aqueous route with L-cysteine (L-Cys) as the capping ligands [36]. Tan et al. synthesized NIR-emitting PbSe QDs with controlled size and shape, with tunable emission in the range from 1200 to 1500 nm. The cell viability of mouse fibroblast cells and human liver cancer cells was retained at 80% even in the presence of a silica shell coated QD loading of 100 $\mu\text{g}/\text{mL}$ [37]. Nanohybrid Au nanoclusters (NCs) -PbS-QDs was synthesized by the co-template method to obtain the NIR-far red dual emission fluorescence. This material is highly suitable for high-resolution bio-imaging because its emission falls in the 'optical window' of *in vivo* imaging with massive Stokes shift and brilliant separation of two emissions (Figure 3(d)) [38]. High-quality, water-dispersible PbS/CdS/ZnS QDs probe lying within the NIR-II window (1000–1350 nm), which leads to higher penetration depths due to the low extinction coefficient of tissues in this spectral range (Figure 3(c)) [39].

Deng et al. developed a facile and environmental-friendly water-soluble PbS QDs with strong fluorescence in the NIR spectral range 870–1010 nm, by using dihydrolipoic acid (DHLA) as the stabilizer [40]. NIR light-emitting luciferase via a biomineralization process was reported by Ma et al. The finding that luciferase remains active and enables bio-luminescence resonance energy transfer within the Luc8-PbS complex represents a significant advance over previous templated nanomaterial synthesis [41]. Pietryga et al. reported a novel method which takes advantage of the reactivity of PbSe QD surface to produce PbSe/CdSe core/shell QDs [42]. The water-soluble conjugated structures, consisting of magnetic nanoparticles (NPs) connected to PbSe were useful for biological applications such as bio-sensing, detection of cancer cells, and drug delivery [43]. Breast tumor cellular imaging was performed using GST-EGFP-GB1 protein-coated PbS QDs with a dual-emission band of visible (515 nm) and second-NIR fluorescence (1150 nm) [44]. Zamberlan et al. reported the development of QDs that combine the

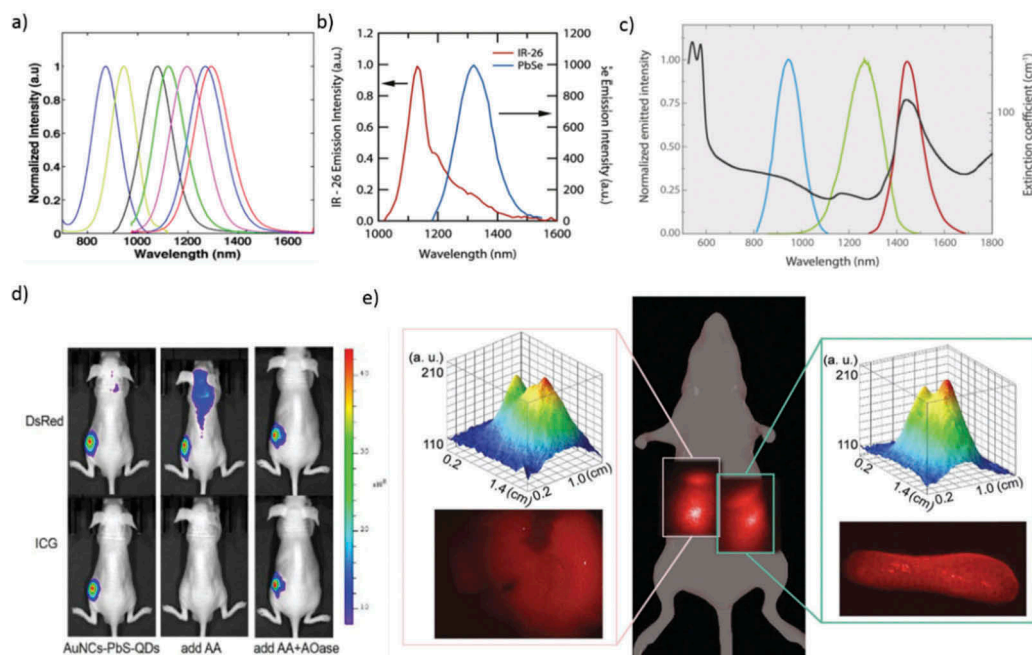


Figure 3. (a) PL spectra of the PbS QDs synthesized by the droplet-based capillary reactor. (b) Comparison of relative PL spectra for IR-26 and a 0.98 eV PbSe QD. (c) The spectral range of different PbS/CdS/ZnS QDs. (d) The nude mice injected with AuNCs-PbS-QDs, AuNCs-PbS-QDs/AA, and AuNCs-PbS-QDs/AA/AOase, respectively. All the images were taken under two filters of DsRed and ICG. (e) Whole body and corresponding intensity surface, and *ex vivo* NIR fluorescence images of the liver (left inset) and spleen (right inset) of a mouse 24 h after tail vein injection of LNH₂ capped QDs. Reproduced with permission from (Figure 3(a), [33] Copyright 2014 The American Chemical Society; Figure 3(b), [32] Copyright 2010 The American Chemical Society; Figure 3(c), [39] Copyright 2015 Wiley Publishing; Figure 3(d), [38] Copyright 2015 The American Chemical Society; and Figure 3(e), [45] Copyright 2018 RSC Publishing).

beneficial bio-compatibility and stability offered by DHLA-PEG-ligands with the tunability of the emission of PbS QDs in the NIR range of low absorption of biological tissues (Figure 3(e)) [45]. Recently, PbS QDs were prepared in sizes between 2.4 and 3.2 nm using PbCl₂, elemental S, dodecanethiol, and a toluene/oleylamine mixture at low temperatures [46].

2.3. Group I-VI quantum dots

Gui et al. reported a facile synthesis of Ag₂S QDs, which exhibit the size-dependent PL bands peaking in the NIR-II region, by cation exchange between visible-emitting CdS QDs and Ag⁺ ions in aqueous solution. Ag₂S QDs produced minor effects on the aspects of altering cell proliferation and generating reactive oxygen species, indicating their ultralow cytotoxicity and excellent bio-compatibility [47]. Tang et al. reported the blood clearance, distribution, transformation, excretion, and toxicity of Ag₂Se QDs modified with polyethylene glycol (PEG) in mice after intravenous injection. The PEGylated Ag₂Se QDs prefers to accumulate in the spleen and liver but is almost transformed and cleared within 1 day. Remarkably, Ag released from the PEGylated Ag₂Se QDs is excreted through both feces and urine, while the important element Se is barely excreted. Finally, the PEGylated Ag₂Se QDs shows low

toxicity, high performance, and proper bio-safety (Figure 4(e)) [48]. Hydrophilic Ag₂S QDs hold great potential for *in vivo* imaging. Recently, Javidi et al. carried out cytotoxicity tests on human A549 and Hep G2 cell lines at concentrations of 6.25–200 μg/ml. The cytotoxicity test revealed that the QDs showed no substantial toxicity. *In vivo* imaging revealed that the Ag₂S QDs penetrated the body of mice with excellent brightness. The water-soluble Ag₂S QDs can be applied as NIR bio-imaging probes for diagnostics or *in vivo* imaging [49].

Song et al. demonstrated a method for preparing ternary AgInS₂, quaternary AgZnInS, AgInS₂/ZnS, and AgZnInS/ZnS nano compounds based on cation exchange. The photostability and *in vitro* experiment confirmed low cytotoxicity and extraordinarily promising applications in the arena of clinical diagnosis [50]. Ag₂Te QDs and Ag₂Te/ZnS core/shell QDs emitting in the NIR-II window ($\lambda_{em} = 900$ –1300 nm) have been reported. These QDs possess small size (~7.6 nm) and are nontoxic to cells, which is perfect for optical bio-imaging [51]. Ag₂Se QDs with tunable PL bands peaking in the NIR-II window ($\lambda_{em} = 1000$ –1400 nm) have been produced by nucleation and growth using 1-octanethiol, a soft Lewis base, as a ligand (Figure 4(a)). The acquired Ag₂Se QDs delivered tunable NIR-II fluorescence in the range from 1080 to 1330 nm. Ag₂Se QDs had excellent fluorescence properties in water, which was

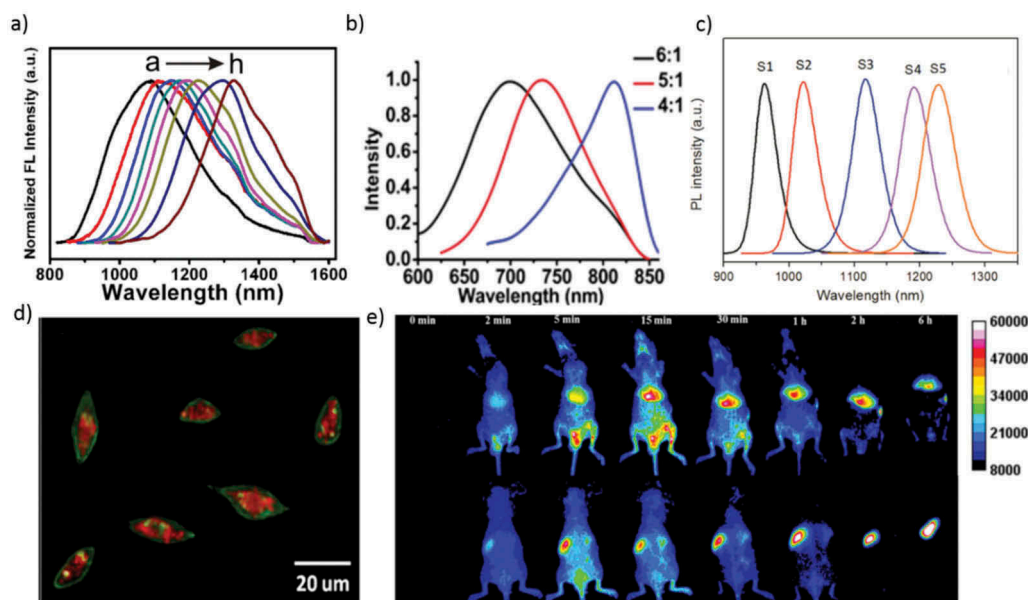


Figure 4. (a) PL spectra of Ag_2Se QDs with different reaction times (b) PL spectra of monodispersed Ag_2Se QDs with different sizes (molar ratio of Ag: Se = 6:1, 5:1, and 4:1). (c) Emission spectra of Ag_2Se QDs capped with a multidentate polymer (samples S1–S5 corresponding to 0.5, 1, 1.5, 2, and 3 h reaction). (d) Overlay image (confocal laser scanning microscopy and NIR) of the Cu-2-[2-chloro-6-hydroxy-5-[(2-methyl-quinolin-8-ylamino)-methyl]-3-oxo-3H-xanthen-9-yl]-benzoic acid (CuFl) stained cells after incubation with the Ag_2S -GSH-SNO NPs for 3 h. (e) *In vivo* imaging of PEGylated Ag_2Se QDs in mice after intravenous injection. (Top row) Abdomen imaging; (bottom row) backside imaging. Reproduced with permission from (Figure 4(a), [52] Copyright 2013 The American Chemical Society; Figure 4(b), [60] Copyright 2012 The American Chemical Society; Figure 4(c), [54] Copyright 2014 The American Chemical Society; Figure 4(d), [53] Copyright 2013 The American Chemical Society; and Figure 4(e), [48] Copyright 2016 The American Chemical Society).

essential for their potential applications in multicolor fluorescence imaging *in vivo* [52].

Tan et al. produced the NIR fluorescent Ag_2S QDs in cultured Hep G2 cancer cells. QD precursors were delivered into the cells, where they reacted to produce QDs under the action of endogenous glutathione. By delivering QD precursors into cultured hepatoma carcinoma cell, Ag_2S QDs with emission efficacy eligible for *in vivo* imaging were effectively synthesized with the aid of endogenous glutathione in the cells (Figure 4(d)) [53]. Later, Tan et al. synthesized Ag_2Se QDs at room temperature with excellent PL QY in the NIR-II region (Figure 4(c)). The results break previous limits in synthetic conditions and provide a low-energy-consuming method for fabricating NIR-II QDs qualified for *in vivo* imaging [54,55]. Ge et al. thoroughly studied the bio-distribution and clearance in mice of NIR ultra-small Ag_2Se QDs. The inductively coupled plasma mass spectrometry (ICP-MS) studies and bio-distribution fluorescent images of Ag_2Se QDs in mouse organs confirmed that the Ag_2Se QDs could be cleared rapidly from the mice body typically by renal excretion without accumulation. Pathological, biochemical analysis, and body weight results also showed that the Ag_2Se QDs do not cause considerable toxicity in the *in vivo* environment [56].

Jiang et al. synthesized emission-tunable NIR Ag_2S QDs with sizes ranging from below 1.5 to 4.6 nm.

The PL spectra cover a range from 690 to 1227 nm, and it has excellent potential for the study of multiple nano-diagnostics and multicolor imaging *in vivo* environment [57]. Dong et al. synthesized Ag_2Se QDs, through a facile solvothermal method with emission centered at 1300 nm. The *in vivo* experiment by administration of C_{18} -PMH-PEG- Ag_2Se QDs by intravenous tail injection attains imaging of organs and vascular structures down to $\sim 100 \mu\text{m}$ [58]. Du et al. showed the combination of different coating ligands and solvents to attaining monodispersed Ag_2S QDs [59]. Gu et al. successfully realize the synthesized water-dispersible Ag_2Se QDs at 90°C with less cytotoxic. The PL emission peak of Ag_2Se QDs has been tuned from 700 to 730 nm and to 820 nm, corresponding to sizes from 1.5 ± 0.4 to 1.6 ± 0.4 nm and to 2.4 ± 0.5 nm with PL QYs more than 1% (Figure 4(b)). The NIR fluorescence of the Ag_2Se QDs can penetrate through a living nude mouse [60].

Zhang et al. developed the bio-conjugation of Ag_2S QDs with particular ligands, targeted labeling and imaging of different cell lines. The Ag_2S QDs had negligible toxicity regarding cell proliferation, apoptosis and necrosis, ROS, and DNA damage. These NIR-II QDs had great potential for *in vivo* imaging, disease finding, and cancer diagnosis with clearance from the body [61]. Zhang et al. studied the long-term *in vivo* bio-distribution of Ag_2S QDs functionalized with PEG and systematically examine

the potential toxicity of Ag₂S QDs overtime. The PEGylated-Ag₂S QDs are accumulated in the liver and spleen after intravenous administration and can be slowly cleared. According to blood biochemistry, hematological analysis, and histological examinations, PEGylated-Ag₂S QDs show slow toxicity when administrated to mice at doses of 15 to 30 mg/kg up to 2 months [62].

Qin et al. synthesized fluorescence-CT dual-mode nanoprobe by making use of DSPE-PEG2000-FA and other amphiphilic molecules to coat Ag₂S QDs and iodinated oil simultaneously. *In vivo* experiments revealed that the probe has a rather long circulation time (blood half-life of 5.7 h), and the histopathological tissue tests indicated that it is not damaging to essential organs normal function [63]. Gui et al. demonstrated a facile aqueous synthesis of Ag₂S QDs (2.6–3.7 nm) with bright and tunable PL emission in a broad range from the red to NIR-II (λ_{em} = 687 to 1096 nm), employing multidentate polymers as capping reagents [64]. Duman et al. established the aqueous synthesis of cationic, NIR-emitting Ag₂S QDs (λ_{em} = 810–840 nm) with a mixed coating of MPA and Polyethylenimine (25 kDa) as new theranostic agent [65,66]. Shi et al. prepared high-quality, NIR-emitting Ag₂Se QDs with distinct absorption features and high PL QYs using ODE–Se as the Se precursor [67]. Theodorou et al. demonstrated significant enhancement of PL intensity in the NIR-II

region for Ag₂S QDs, using Au nanostructures produced by colloidal lithography [68]. Zhang et al. effectively modified Ag₂S QDs with a tumor-targeting small protein, affibody ZEGFR: 1907, via charge interaction. The resulting probe displays an EGFR targeted tumor imaging property, and it has a high potential for bio-imaging [69]. In 2014, Chen et al. prepared Ag₂S QDs conjugated with TAT peptide in the second NIR window (NIR-II, 1.0–1.4 μ m) for dynamically tracking of human mesenchymal stem cells *in vivo* with high sensitivity and high spatial and temporal resolution [70]. Recently, Chen et al. reviewed and discussed tracking the transplanted stem cells using fluorescent nanoprobes in the first and second biological window [71].

2.4. Group I-III-VI quantum dots

Recently, researchers concentrated on I–III–VI₂ group semiconductor NPs of Cu or Ag-based materials, such as CuInS₂, Cu(In,Ga)Se₂, and AgInS₂, due to their low toxicity [72]. Mao et al. synthesized the NIR-emitting AgInS₂/ZnS QDs by heating an Ag/In/Zn/S solution and ending the reaction at 165 °C. Zinc concentration and rising temperature played significant roles in the formation of the NIR-emitting QDs (Figure 5(c)). Zinc enables the growth of the AgInS₂/ZnS NCs at elevated temperatures without aggregation, and it suppresses the formation

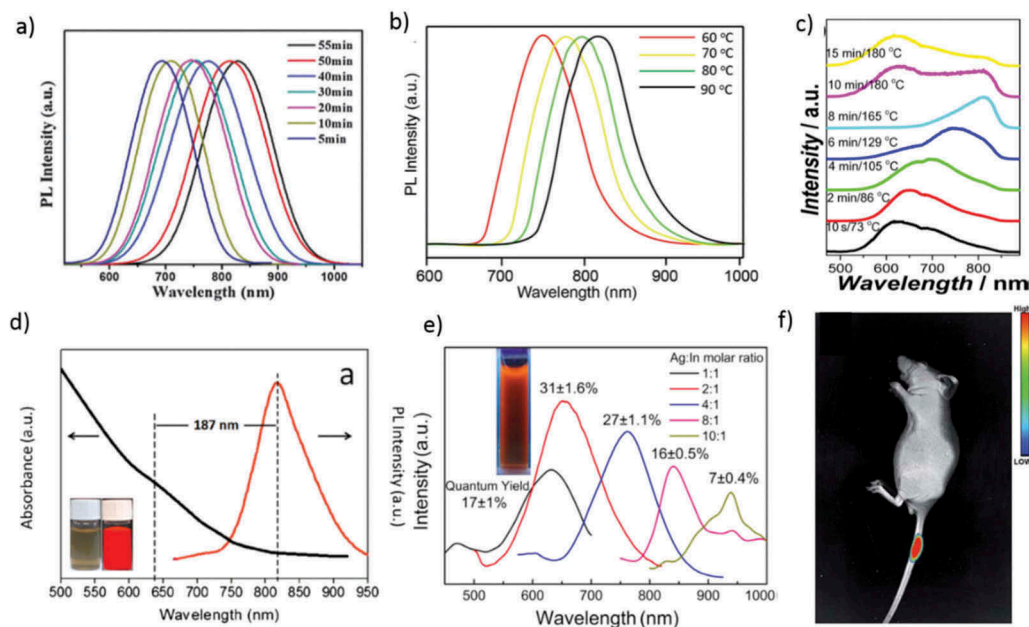


Figure 5. (a) The PL spectra of CuInS₂ QDs at different reaction times. (b) PL spectra of RNase A-CuInS₂ QDs at different reaction temperatures. (c) PL spectra of AgInS₂/ZnS NCs by heating the Ag/In/Zn/S (1:1:0.5:2.5) solution from 90 to 180 °C. (d) Vis–NIR absorption and PL spectra of AgInS₂ QDs capped with a multidentate polymer synthesized for 105 min; (inset) bright-field image and PL image in pseudocolor. (e) PL spectra of AgInSe₂ QDs prepared with different Ag:In molar ratios. The inset shows AgInSe₂ QDs (Ag:In molar ratio of 2:1) in water, excited with a UV lamp at 365 nm. (f) Mice after treatment with the RNase A-CuInS₂ QDs. Reproduced with permission from (Figure 5(a), [80] Copyright 2016 RSC Publishing; Figure 5(b), [74] Copyright 2017 RSC Publishing; Figure 5(c), [73] Copyright 2014 The American Chemical Society; Figure 5(d), [76] Copyright 2015 Elsevier publishing; Figure 5(e), [78] Copyright 2016 Elsevier publishing; and Figure 5(f), [74] Copyright 2017 RSC Publishing).

of defects which leads to an enhancement of the PL intensity of AgInS₂/ZnS QDs. The beautiful NIR-emitting properties of the AgInS₂/ZnS NCs make them potentially desirable for bio-imaging applications [73].

Xi et al. demonstrated a one-pot synthesis of water-soluble, NIR-emitting CuInS₂ QDs using RNase A for *in vivo* imaging experiment; this result confirmed that they could be a good candidate for biomedical applications, particularly in the gastrointestinal system (Figure 5(b,f)) [74]. Jiang et al. synthesized Cu-doped Zn-In-S QDs by a hydrothermal method for labeling Hep G2 liver cancer cells. The cytotoxicity studies revealed that the viabilities of the cells incubated with increasing concentrations of CZIS/ZnS QDs all remained at a high level of more than 90%. Hence, the CZIS/ZnS NP is a promising material as the fluorescent probe for biological applications [75]. Tan et al. demonstrated water-dispersible AgInS₂ QDs with bright NIR emission (Figure 5(d)). A type of multidentate polymer was synthesized and utilized as a compact capping ligand for the AgInS₂ QDs. The multidentate polymer capping AgInS₂ QDs are highly luminescent in the NIR window and have high photostability. Also, the QDs are stable in various media and have low cytotoxicity. Nude mice photoluminescence imaging shows that the multidentate polymer capping AgInS₂ QDs can be well applied to *in vivo* imaging. These NIR fluorescent QDs have great potential for bio-medical applications [76].

Fahmi et al. prepared water-soluble AgInS₂-ZnS QDs covered by oleylamine without surfactant or polymer for cancer cell staining. To demonstrate the targeting capability, folic acid was further conjugated with oleylamine encapsulated AgInS₂-ZnS QDs for HeLa and MCF7 cancer cell staining [77]. Recently, a fast and straightforward synthesis of strongly NIR-luminescent AgInSe₂-ZnSe QDs with tunable emissions in aqueous media has been reported. This method avoids high temperature and pressure and organic solvents to produce water-soluble AgInSe₂-ZnSe QDs. The PL peaks of the AgInSe₂-ZnSe QDs could be controlled in the ranging from 625 to 940 nm, along with PL QYs of 31% at maximum (Figure 5(e)). So, the AgInSe₂-ZnSe QDs with high PL QY, emission tunability in the NIR range and low cytotoxicity are useful for cell labeling and bio-imaging [78]. Liu et al. reported highly water-soluble quality ternary CuInS₂ QDs with MPA ligands as a stabilizer. They were used to label the liver cancer cells [79]. Qi et al. reported CuInS₂ QDs with tunable emission from visible to NIR range ($\lambda_{em} = 675-835$ nm), the PL QYs of up to 8.7% were observed by just controlling the reaction time (Figure 5(a)) [80].

2.5. Group III-V quantum dots

High-quality InAs QDs are likely the best candidate for NIR-light emitters ($\lambda_{em} = 700-1400$ nm) among

II-VI, III-V, and IV-VI semiconductor QDs. InAs QDs with NIR-emitting properties were synthesized through a self-focusing of size distribution. One-pot synthesis can yield core-shell QDs with bright (up to 90% PL QY), stable, and narrow NIR-PL spectra, which is preferred for *in vivo* bio-medical imaging. Cu-doped InP QDs were successfully synthesized by epitaxial growth of a ZnSe diffusion barrier for the dopants. The Cu-dopant emission of the Cu: InP/ZnSe core/shell QDs covers a broad PL range from 630 to 1100 nm, and emission tunability is achieved by varying the size of the InP core (Figure 6(b)) [81].

Allen et al. prepared water-soluble InAs (ZnCdS) QDs with bright and stable PL bands peaking in the NIR region (Figure 6(c)). The NIR-emitting QDs can be functionalized to allow imaging of exact cellular proteins. Also, the efficacy of the NIR region for *in vivo* imaging is proved by the greater ability of InAs (ZnCdS) QDs to image tumor vasculature [82]. Colloidal III-V semiconductor QDs are well focused because of rich phenomena related to the effect of quantum confinement. However, studies of III-V QDs are limited due to synthetic complications. High-quality InP QDs has been adequately developed as luminescence probes for bio-imaging (Figure 6(a)) [83]. Bruns et al. introduced the short-wavelength infrared region (SWIR)-emitting InAs-based core-shell and core-shell-shell QDs as a flexible class of materials for functional biological imaging. These InAs-based QDs display higher QY and stability than previously described SWIR probes [84]. Gao et al. reported using 22B and LS174T tumor xenograft models, *in vivo* and *ex vivo* imaging studies show that QD800-MPA is hugely accumulated in the tumor part, which is essential for tumor detection in living mice (Figure 6(d)) [85].

2.6. Group IV quantum dots

It is a special kind of QDs based on only one element. Carbon dots (CDs) attracted much attention [86-91]. Zheng et al. reported NIR fluorescent Cy (cyanine dye) CD by the reaction of CyOH with PEG800 which is excellent photostability and biocompatibility. CyCD gives strong absorption around 600 to 900 nm, NIR emission for *in vivo* imaging, favored uptake, and accumulation at tumors [92]. Pan et al. reported the CD fluorescent probes that are excited with NIR light to give a NIR emission. The red-emitting CD ($\lambda_{max} = 683$ nm) could be excited with an 850 nm light from a femtosecond pulsed laser. The NIR-emitting CDs exhibit an excellent water solubility, a narrow spectral emission, and high PL QY that is high as 16.8%. More remarkably, the NIR-emitting CDs have low cytotoxicity and are adapted for two-photon excitation. These CDs could not only be potentially employed for deep tissue two-photon excitation

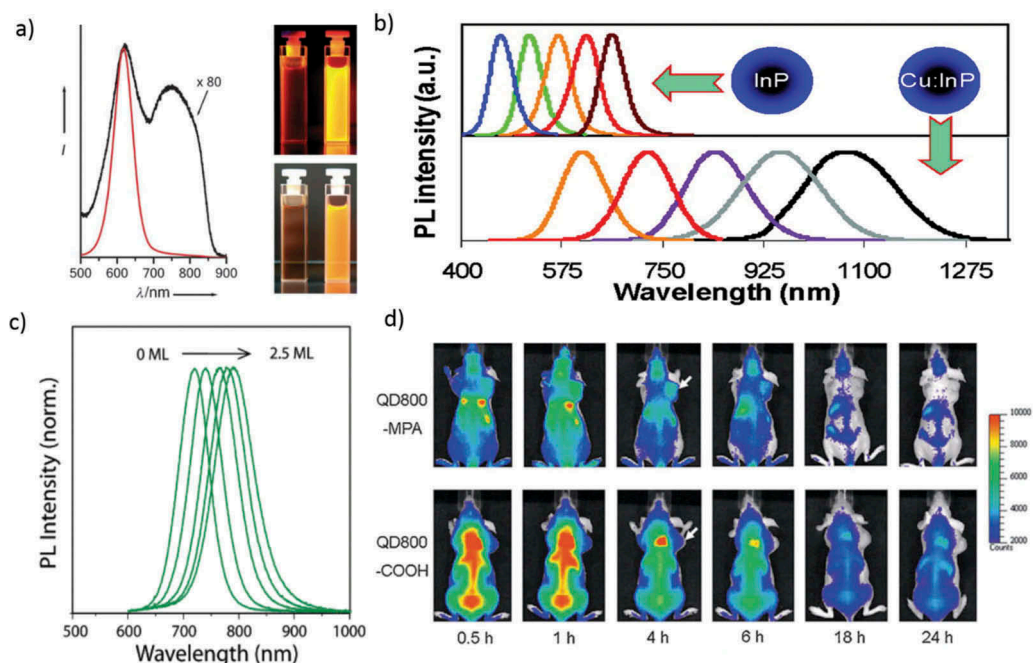


Figure 6. (a) PL spectra of InP QDs grown at 250 °C for 4 h before (black line) and after (red line) HF etching. Photographs of both colloidal solutions under UV illumination (inset top-366 nm) and UV/white light flash (inset bottom). (b) PL spectra of differently sized InP QDs and Cu: InP d-dots (c) PL of InAs ($\text{Zn}_{0.7}\text{Cd}_{0.3}\text{S}$) during shell growth from 0–2.5 monolayers. (d) *In vivo*, NIR fluorescence imaging of 22B tumor-bearing mice (arrows) injected with QD800-MPA and QD800-COOH, respectively. Reproduced with permission from (Figure 6(a), [83] Copyright 2008 Wiley Publishing; Figure 6(b), [81] Copyright 2014 The American Chemical Society; Figure 6(c), [82] Copyright 2010 The American Chemical Society; and Figure 6(d), [85] Copyright 2010 Wiley Publishing).

bio-imaging but also used as a carrier for the delivery of drugs that cannot enter into living cells directly [93]. Li et al. successfully prepared NIR-emitting CDs (R-CDs) using spinach as a precursor. The R-CDs showed an excellent water solubility, a remarkable photo-stability, an emission peak at 680 nm, a 15.34% PL QY, excellent compatibility, and low toxicity. R-CDs were proved to have excellent cellular labeling agent with lung cancer cells (A549) excited at 543 nm [94].

Lan et al. prepared CDs codoped with S, Se via a hydrothermal method and NIR emissions of the CDs, with PL bands peaking at 731 and 820 nm and photothermal conversion efficiency of ~58.2%. The two-photon absorption cross-section ($\sim 30,045 \text{ GM}$; $1 \text{ GM} = 10^{-50} \text{ cm}^4 \cdot \text{s}/\text{photon}$) of the CDs are high enough to give a NIR emission. *In vitro* and *in vivo* tests suggested that CDs are useful phototheranostic agents for the two-photon excitation fluorescence imaging and photothermal therapy of cancer cells [95]. Li et al. showed that surface modified CDs could absorb the light for NIR emission. CDs in dimethyl sulfoxide (DMSO) exhibit an absorption band in the NIR-I region at 715 nm and NIR emission at 760 nm (PL QY reaching 10%), under NIR excitation. The NIR excitation and emission are both critical for CDs to realize the *in vivo* fluorescence imaging. Besides, two-photon and three-photon-induced fluorescence are observed in DMSO under

excitation of light peaking in the NIR-II window. CDs modified with Poly(vinylpyrrolidone) (PVP) are used in the stomach of a living mouse for *in vivo* NIR fluorescence imaging. This is the first approach to get CDs with a NIR absorption band and NIR emissive CDs efficiently with either one-photon excitation in a NIR-I or multiphoton excitation in a NIR-II window for applications in NIR fluorescence imaging (Figure 7(d,e)) [96,97].

Group-IV QDs have recently attracted attention as a nontoxic alternative to classical II-VI and IV-VI QDs containing toxic elements such as Hg, Cd, and Pb. Bulk crystal of Ge is a typical indirect bandgap semiconductor with a narrow bandgap of 0.7 eV at room temperature and exhibits a poor optical performance because of its indirect bandgap character. However, the carrier confinement in an NP of Ge crystal with a diameter smaller than the bulk exciton Bohr radius ($\sim 11.6 \text{ nm}$) alters the energy structure. This situation allows for the overlapped wave functions of spatially confined carriers, leading to zero-phonon optical inter-band transitions for recombination as a result of the relaxation of the k-selection rule due to the Heisenberg uncertainty relation. After the 1993 report on yellow-emitting Ge QDs, it was found that control over size and structure of CDs results in emission tunability over the entire visible wavelength range [98–100].

In contrast, a few papers report the fluorescence colors in the NIR wavelength region [101–103].

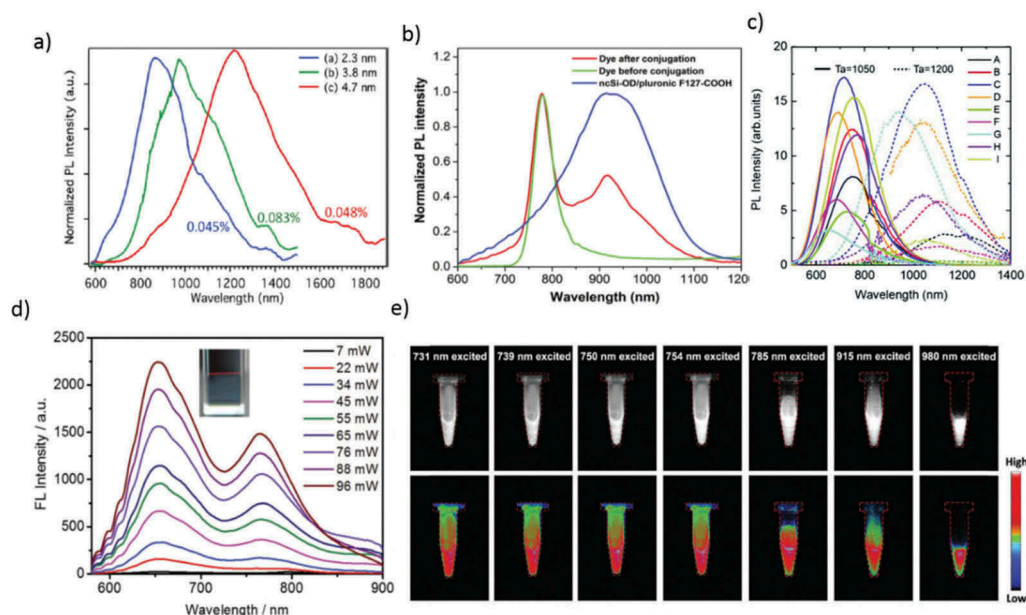


Figure 7. (a) PL spectra of tetrachloroethylene solutions of Ge-NC (100/0), Ge-NC (0/100), and Ge-NC (50/50) under 405 nm excitation. PL QY values are shown in percentage. (b) Normalized PL spectra of NCSi-OD/F127-COOH, HiLyte Fluor 750 amine dye and NCSi-OD/F127-COOH conjugated with the dye when excited at 350 nm. (c) PL spectra of a colloidal solution of codoped Si QDs. The growth temperatures are 1050 (solid) and 1200 °C (dashed). (d) Fluorescence spectra obtained for multiphoton excitation associated with incident intensities at; 1200 nm excitation (inset: excitation at 1200 nm and 22 mW). (e) SWIR fluorescence images of FCDs in aqueous dispersions, excited by lasers and captured with an InGaAs camera. Images in the bottom row are the heat maps of those in the upper row. Reproduced with permission from (Figure 7(a), [104] Copyright 2010 The American Chemical Society; Figure 7(b), [107] Copyright 2016 RSC Publishing; Figure 7(c), [141] Copyright 2016 RSC Publishing; Figure 7(d), [97] Copyright 2018 RSC Publishing; and Figure 7(e), [96] Copyright 2018 RSC Publishing).

Ruddy et al. synthesized, alkyl-terminated Ge QDs (2.3–11.3 nm) based on the reduction of $\text{GeI}_4/\text{GeI}_2$ mixtures. The NIR absorption (1.60–0.70 eV) and corresponding band-edge emission demonstrate the highly tunable quantum confinement effects in Ge QDs prepared using this mixed-valence precursor method (Figure 7(a)) [104]. Continuous tunability was achieved in a biological window of 900–1600 nm. However, the emission QY is still too low (~5%) for fluorescence biomarkers.

Bulk crystalline silicon (Si) is also included in a category of indirect bandgap semiconductors with a bandgap of 1.1 eV at room temperature. It is broadly known that the electronic structure in Si QD retains its indirect bandgap character. The effects of quantum confinement lead to the relaxation of the momentum conservation by the uncertainty principle ($\Delta\chi\Delta\rho \geq \hbar/2$), which allows for zero-phonon optical interband transitions. This theory predicts the appearance of PL peaks tailing on a low energy side. This tailing continues until ~1.1 eV, which is equal to the value of the bulk bandgap for crystalline Si. However, most of NIR PL spectra reported recently show homogeneous and Gaussian-like shape without long emission tails [105]. Although the PL QYs of the hydrogen-terminated Si QD are as low as ~5%, a merely substituting their surface hydrogen atoms with alkyl chains, which yields a covalent carbon-silicon linkage, increases the PL QYs up to ~70% [106].

Furthermore, the size-dependency of PL peak energy is achieved even after substitution of the surface ligands [107]. Presently, the high PL QY is postulated to arise from an increase in the radiative recombination rate [108], a dramatic reduction of the non-radiative channels [109,110], or a bandgap modulation from indirect to direct transitions [111]. Such an enhancement of PL QYs has been arguably observed for alkyl-terminated QDs with size-dependent PL bands and encourages the further development of QD-based optoelectronics devices [112–114].

Furthermore, Si QDs are nontoxic, easy availability, a long PL lifetime on μs scale, along with brightness and it give fluorescence emission from UV to NIR wavelength range (Figure 7(b)) [115–124]. NIR-emitting Si QDs have been prepared by non-thermal Plasma or thermal disproportionation of hydrogen silsesquioxane ($\text{HSiO}_{1.5}$), followed by hydrofluoric etching to liberate the Si QDs from the oxide matrix [125–127]. In most of the studies, $\text{HSiO}_{1.5}$ purchased from Dow Corning (trade name FOx-17) are used for QD synthesis [128,129], but a similar compound could be derived from the hydrolysis of trichlorosilane or triethoxysilane [130,131]. Impurity doping of boron, phosphorus, or transition metals into diamond cubic Si lattice has also been achieved [132,133]. Sugimoto et al. developed a new approach for the formation of all-inorganic Si QDs that are codoped with boron and phosphorus with excellent stability in water without

organic ligands, exhibit bright and stable luminescence in the NIR wavelength range [134]. Wang et al. reported for the first time the bio-medical use of Si QDs as a fluorescence label to DNA [135]. Since then, Swihart and co-workers have significantly developed this research field [136]. As the cytotoxicity is strongly influenced by surface terminal groups [137,138], the amphiphilic molecules such as Pluronic F127 or PEG are frequently employed for encapsulating the core of Si QDs, yielding the high hydrophilicity and biocompatibility. Si QDs exhibit a low absorption efficiency to the red-to-NIR lights. Therefore, it is difficult to attain the NIR-NIR excitation-emission bio-imaging in the single-photon excitation environment. To overcome this difficulty, He et al. reported possible compatibility of multiphoton excitation technique with Si QD [139]. Chandra et al. developed water-borne Si QD adapted for 2-photon excitation and used it to provide for the first time direct evidence of the NIR-NIR excitation-emission imaging [107]. Ravotto et al. presented a light-harvesting two-photon antenna using the emission of Si QDs. This result opens up the potential for bio-imaging applications, such as deep tissue imaging, high resolution, and low photodamage, coupled with the bright, long-lived, and oxygen-insensitive NIR luminescence of Si QDs [140]. Recently, Sakiyama et al. developed a long-lived luminescence of colloidal silicon QDs for time-gated fluorescence imaging in the second NIR window in biological tissue (Figure 7(c)) [141].

2.7. Sentinel lymph node mapping using NIR QDs

Tumor metastasis usually occurs through the lymphatic or hematogenous pathway [142]. Therefore, the identification of metastasis within the sentinel lymph nodes (SLNs) is most important. Figure 8(a) outlines SLN mapping using nanoscale imaging probes with different sizes [143,144]. In 2004, Kim et al. reported type II NIR QDs with a polydentate phosphine coating for SLN mapping in both small and large animals. Injection of only 400 pmol of NIR QDs permits sentinel lymph nodes 1 cm deep to be imaged easily in real time using excitation intensity of only 5 mW/cm² [145]. CdSe/ZnS core/shell QDs emitting around 655 nm was used for detection of axillary lymph node (ALN) as soon as 5 min and up to 24 h after the injection (Figure 8(b)). The maximum amount of QDs in the ALN was detected 60 min after the injection and corresponded to 2.42% of the injected dose. Most of the injected QDs remained at the injection site. No QDs were detected in other tissues, plasma, urine, and feces [146]. CdTe/CdS QDs are conjugating with *R. reniformis* luciferase (Luc8) used for *in vivo* SLN mapping because of their high sensitivity resulting from the limited background interference, as well as the high depth of tissue penetration of the luminescence [147]. Si

et al. used cadmium tellurium QDs in rats for *in vivo* lymph node mapping. Both methylene blue and QD stained the sentinel lymph node quickly, but methylene blue was challenging to identify in the deep tissues and the LNs beyond the SLN. Furthermore, the blue-stained LNs remain dyed for only 2 h. In contrast, the QDs exhibited high target-to-background ratios in both the SLNs and the following LNs [148]. In 2010, Pons et al. used cadmium-free CuInS₂/ZnS QDs for sentinel lymph node (LN) imaging with reduced toxicity. They used bright and photostable core/shell CuInS₂/ZnS QDs with emission ranging from the red to NIR using air-stable compounds. After the water-soluble process, the QDs are used *in vivo* imaging of two regional LNs draining thoracic mammary fat pads in mice. The comparison of dose-dependent inflammatory response in the regional LNs induced by NIR CdTe-Se/CdZnS and CuInS₂/ZnS functionalized with the same surface chemistry and show that CuInS₂/ZnS presents a much-reduced toxicity compared to Cd-based QDs [149]. One year later, Erogbogbo et al. used bio-compatible silicon nanocrystals for sentinel lymph node mapping in live mice. When injected subcutaneously in the paw of a mouse, MSiQDs traveled through the lymphatics and migrated to an axillary location (Figure 8(c)) [150].

2.8. Advantages and disadvantages of NIR QDs

Cd-based QDs have been primarily used for bio-imaging based on their high quantum efficiencies. The high brightness and stability of PL of QDs are favorable for medical applications such as a fluorescence image-guided surgery for tumor removal. However, those QDs are made of CdSe and have cadmium selenide core with zinc sulfide shell (CdSe/ZnS), containing inherently toxic cadmium. Table 2 shows a summary of the toxicity studies of various types of QDs [136]. A variety of *in vivo* models are demonstrated for each assessment. As expected, QDs containing Cd and Pb show high toxicity in every case. High cytotoxicity of Ag₂Se QD comes as a surprise although they show a good NIR PL performance based on the effect of quantum confinement. These advantages in PL performance offered by the QDs cannot outweigh the potential risk associated with the accumulation of their constituent elements in the human body.

In Table 2, PbSe are non-toxic until 100 µg/mL. It can be predicted that PbS also show a similar assessment of toxicity. PbS/SiO₂ core-shell QDs are non-toxic until 220 µg/mL in cell culture due to the presence of the nontoxic shell, and this amount is as high as that of Si QD. It is noted that the amount for the availability of the PbS/SiO₂ QD is very less for nonhuman primate study of QD toxicity. However, Si QD demonstrates the non-toxicity even at 380 mg/kg which is 15 times larger than the limitation of the PbS/SiO₂ QD (~25 mg/kg).

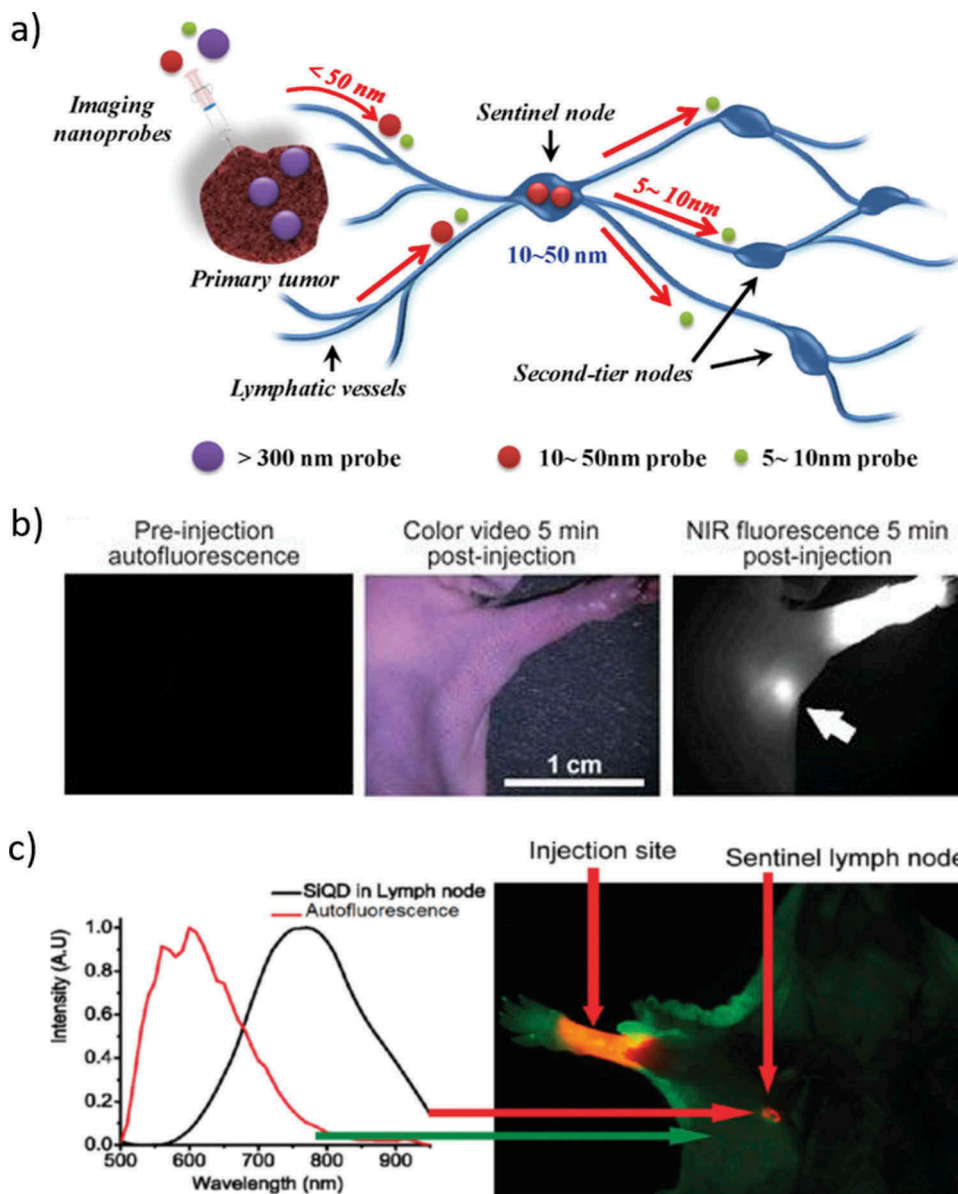


Figure 8. a). Schematic illustration of SLN mapping using a nanoscale imaging probe. Imaging probes on the 5–10 nm size scale can flow through the SLN into adjacent nodes in the chain; nanoprobe >300 nm in size rarely leave the injection site. Nanoprobes with a hydrodynamic diameter of 10–50 nm exhibit rapid uptake into SLN and do not leave. b). NIR QD sentinel lymph node mapping in the mouse; Images of mouse injected intradermally with 10 pmol of NIR QDs in the left paw. Left, pre-injection NIR autofluorescence image; middle, 5 min post-injection white light color video image; right, 5 min post-injection NIR fluorescence image. An arrow indicates the putative axillary sentinel lymph node. Fluorescence images have identical exposure times and normalization. c). Sentinel lymph node imaging following localization of Si QDs in an axillary position. Autofluorescence is coded in green, and the unmixed Si QD signal is coded in red. Reproduced with permission from (Figure 8(a), [143] Copyright 2012 The American Chemical Society; Figure 8(b), [145] Copyright 2004 Nature Publishing Group; and Figure 8(c), [150] Copyright 2011 The American Chemical Society).

This comparison suggests that covering the toxic cores with less-toxic materials could not be the answer to solve the problems. In addition, the presence of heavy-metals in these QDs makes them a potential risk to the environment as their use increases and products reach the end of life. Pb-based QDs also emit high-intensity light up to second near infra-red region; researchers were used in lower concentration for bio-imaging after surface modification.

Many papers report that Ag-based QDs are a non-toxic probe for cells which is emitted light in

the second infrared region. Ag₂S QDs may be better than Cd, Pb, and Hg although more careful assessment is necessary. CuInS₂ and AgInS₂ QDs are much more bio-compatible than toxic QDs like HgTe, CdHgTe, CdTeSe, CdTeSe/CdS, PbS, and Au/PbS QDs. InAs-based core-shell QDs does not show high cytotoxicity and rapidly eliminated through renal clearance which reduces potential toxicity to the body. Si and Ge QDs are non-toxic to the human body, and it will emit the light in the near infra-red region. For Si QDs, the drawback is low

Table 2. Different types of quantum dots used for *in vivo* toxicity studies in various animal models. Copyright 2013, Royal Society Of Chemistry. Reproduced with permission from Yong et al. [136].

Type of QD	Cells	Zebrafish	Xenopus embryo	Mouse	Rat	Macaque
CdSe	Toxic after oxidation, ~0.0625 mg ml ⁻¹	-	-	-	-	-
CdSe-ZnS ^a	Toxic after exposed to UV irradiation, ~1 mg ml ⁻¹	LC ₅₀ values: 7–42 μM	Non-toxic at 4.2X10 ⁹ particles per cell	Non-toxic at 360 pmol- 6 nmol	Non-toxic at 15 nmol	-
CdSe-CdS-ZnS ^b	LC ₅₀ : ~0.7 μM	-	-	Non-toxic at 125 nmol	Non-toxic at 3 nmol	Non-toxic at 25 mg kg ⁻¹
CdSe-CdS	LC ₅₀ : 50–100 nM	-	-	Non-toxic at 48 pmol	-	-
CdTe	LC ₅₀ : ~ 40 μg/mL	-	-	-	-	-
CdTe-ZnSe	Non-toxic at 1 mg ml ⁻¹	-	-	Non-toxic at 5 mg kg ⁻¹	-	-
CdTe-ZnTe	Relatively Non-toxic at 150 μg ml ⁻¹	-	-	Non-toxic at 5 mg kg ⁻¹	-	-
CdTe-CdS-ZnS	Non-toxic at 3.0 μM	-	-	-	-	-
CdHgTe-ZnS	Adopted for cell imaging, no toxicity study was performed	-	-	-	-	-
CdSe-CdTe	Non-toxic at 1–10 μg ml ⁻¹ loaded in PLGA nanospheres	-	-	Sentinel lymph node mapping in mouse (dosage ~0.01 nmol) and pig (dosage ~0.4 nmol), no toxicity study was performed	-	-
CdTe _x Se _{1-x} -CdS	Non-toxic at 200 μM	-	-	Nontoxic at 5 mg kg ⁻¹	-	-
InP-ZnS	Non-toxic at 100 mg ml ⁻¹	-	-	Intratumor administration of 74 μg for imaging, no toxicity study was performed	-	-
Mn:ZnSe	Non-toxic at 1.2 μM	-	-	-	-	-
ZnS:Mn-ZnS	Non-toxic at 400 μg ml ⁻¹	-	-	Non-toxic at 0.5 mg	-	-
Mn:CdSe _x Te _{1-x} -CdS	Non-toxic at 800 μg ml ⁻¹	-	-	Non-toxic at 10 mg kg ⁻¹	-	-
InAs _x P _{1-x} -InP-ZnSe	-	-	-	Non-toxic at 150 pmol	-	-
InAs-ZnSe	-	-	-	Used for imaging, no toxicity study was performed	Sentinel lymph node imaging, no toxicity study was performed	-
InAs-InP-ZnSe	LC ₅₀ : ~100 nmol L ⁻¹	-	-	Non-toxic at 0.5 nmol	-	-
CuInSe ₂	-	-	-	Sentinel lymph node imaging, no toxicity study was performed	-	-
CuInS ₂	LC ₅₀ : ~300 mg ml ⁻¹	-	-	Non-toxic at 0.1–0.2 μmol (based on Cu atoms), or 0.5 mg	-	-
Ag ₂ Se	Non-toxic at 47.4 μg ml ⁻¹	-	-	Non-toxic at 0.15 mg	-	-
PbSe	Non-toxic at 100 μg ml ⁻¹	-	-	-	-	-
PbS	Non-toxic at 220 μg ml ⁻¹	Caused	Malformations above 40 μg ml ⁻¹	-	Non-toxic at 25 mg kg ⁻¹ or 0.3 mg	-
ZnS	Non-toxic at 100 μM	-	-	-	-	-
Si	Non-toxic at 0.2 mg ml ⁻¹	-	-	Non-toxic at 380 mg kg ⁻¹ or 60 nmol	-	-
CdSe-CdS	LC ₅₀ : less than 500 μM	-	-	-	-	-
Quantum rods	-	-	-	-	-	-
CdSe-CdS-ZnS	Non-toxic at 500 μM	-	-	Non-toxic at 1 mg	-	-
Quantum rods	and 2.8 μg ml ⁻¹	-	-	-	-	-

^aCore-shell structure. ^bCore-shell-shell structure

photoabsorption coefficient because of their energy structure that retains indirect bandgap nature

observed for bulky crystal. Surface chemistry is allowing the efficient fluorescence resonance energy

transfer between surface ligands working as absorbers and Si QDs is expected to solve this problem. For Ge NCs, the PL QY should be increased.

3. Summary and perspectives

In this review, we summarized recent progress in biomarkers of NIR-emitting QDs for fluorescence bio-imaging. The review focuses on the tremendous efforts invested in the colloidal synthesis and functionalization of the water-borne NIR-emitting-QDs with different chemical compositions. Especially, we outlined the applications of NIR-QDs in the area of *in vitro* and *in vivo* imaging, using their unique optical properties, low toxicity, surface functionalization, high photostability and brightness. Besides, we summarized the *in vivo* fluorescence imaging of sentinel lymph node and tumors. Thanks for the variety of constantly evolving synthetic strategy for colloidal QDs and their improved optical performance, there are many possible QDs at present, which exhibit high stability in an aqueous buffer solution, a broad wavelength tunability in the biological window, and a significantly improved PL QY. Recent studies for the NIR-emitting QDs of IV, I-VI, II-VI, IV-VI, III-V, and I-III-VI semiconductors are picked up to be demonstrated herein. By controlling the size of their QDs, the accessible emission wavelength for bio-imaging is extended to the NIR-I and NIR-II window. Furthermore, the QDs shown have a unique optical performance such as a large multiphoton absorbance cross-section, yielding a multiphoton absorption of NIR light to result in the successful multiphoton imaging and an unconverted emission imaging. According to this scenario, synthesis and optical performance of NIR-emitting Cd-, Pb and Hg-based QDs are also described although their toxicities are known well. According to the scenario demonstrated in Table 2 reports the encapsulation of these toxic QDs with SiO₂ or polymers, but the covering the toxic cores with less-toxic materials could not be the answer to solve the cytotoxic problems. QDs with diameters larger than dye-molecules enables chemists to access to the photoacoustic imaging due to larger vibration of their crystalline lattice structures. Meanwhile, IV QDs such as C, Si, and Ge provide advantages in terms of ultralow cytotoxicity, biocompatibility and the ability to form a covalent linkage with organic ligands, resulting in high stability even in the aqueous buffer containing bovine serum albumin. In particular, Si is an abundant element and takes advantage of its high QY greater than 60%. As QDs of Si and Ge provide a long PL lifetime on μ sec scale, biochemists can avoid the unwanted effect of autofluorescence from cell molecules on bio-imaging, and meet a good opportunity to be accessible to time-gated bio-imaging. Moreover, the low toxicity of Si and Ge QDs has relieved some of the concerns associated with

their use *in vivo* environment. Further investigations of the toxicological impacts and bio-friendly surface chemistry in different biological models are needed, but these distinguishing features observed in the NIR-emitting QDs can expand their use to various pathways for beautiful imaging that includes photothermal cellular imaging under *in vitro* and *in vivo* environment, leading to the next generation concept of nanomedicine ‘Theranostics’ that is a combination of diagnosis and therapy with medical treatments. In the future, we would predict a powerful technique using NIR-QDs for fluorescence *in vivo* imaging in terms of high sensitivity and deep tissue penetration capacity. Alternatively, the synthesis of biocompatible, stable NIR-QDs using green approach is mandated. Also, we need effective synthetic methods to get high quantum efficiency NIR QDs with a narrow full-width half maximum.

Acknowledgments

The authors acknowledge financial support from the WPI Program of the Ministry of Education, Culture, Sports, Science, and Technology (MEXT), Japan. SC was supported by a tenure-track program of NIMS ‘International Center for Young Scientists’ (ICYS). NS appreciates the financial support from JST A-step (AS282I006e) and Izumi Foundation.


Disclosure statement

No potential conflict of interest was reported by the authors.

Funding

This work was supported by the Izumi Science and Technology Foundation [2018-J-053]; Japan Science and Technology Agency [AS282I006e].

ORCID

Shanmugavel Chinnathambi  <http://orcid.org/0000-0001-9550-5367>

Naoto Shirahata  <http://orcid.org/0000-0002-1217-7589>

References

- [1] Michalet X, Pinaud FF, Bentolila LA, et al. Quantum dots for live cells, *in vivo* imaging, and diagnostics. *Science*. 2005;307:538–544.
- [2] Lee SW, Mao C, Flynn CE, et al. Ordering of quantum dots using genetically engineered viruses. *Science*. 2002;296:892–895.
- [3] Li J, Zhu JJ. Quantum dots for fluorescent biosensing and bio-imaging applications. *Analyst*. 2013;138:2506–2515.
- [4] Park Y, Jeonga S, Kim S. Medically translatable quantum dots for biosensing and imaging. *J Photochem Photobiol C*. 2017;30:51–70.

- [5] Martinic I, Eliseeva SV, Petoud S. Near-infrared emitting probes for biological imaging: organic fluorophores, quantum dots, fluorescent proteins, lanthanide (III) complexes and nanomaterials. *J Lumin.* **2017**;189:19–43.
- [6] Gao G, Jiang YW, Sun W, et al. Fluorescent quantum dots for microbial imaging. *Chin Chem Lett.* **2018**;29:1475–1485.
- [7] Pic E, Pons T, Bezdetnaya L, et al. Fluorescence imaging and whole-body biodistribution of near-infrared-emitting quantum dots after subcutaneous injection for regional lymph node mapping in mice. *Mol Imag Biol.* **2010**;12:394–405.
- [8] Alivisatos AP. Semiconductor clusters, nanocrystals, and quantum dots. *Science.* **1996**;271:933–937.
- [9] Liu TM, Conde J, Lipiński T, et al. Revisiting the classification of NIR-absorbing/emitting nanomaterials for in vivo bio applications. *NPG Asia Mater.* **2016**;8:295.
- [10] Hong G, Antaris AL, Dai H. Near-infrared fluorophores for biomedical imaging. *Nat Biomed Eng.* **2017**;1:0010.
- [11] Ding F, Zhan Y, Lu X, et al. Recent advances in near-infrared II fluorophores for multifunctional biomedical imaging. *Chem Sci.* **2018**;9:4370–4380.
- [12] Lu C, Chen G, Yu B, et al. Recent advances of low biological toxicity Ag₂S QDs for biomedical application. *Adv Eng Mater.* **2018**;20:1700940.
- [13] Koch M, Symvoulidis P, Ntziachristos V. Tackling standardization in fluorescence molecular imaging. *Nat Photon.* **2018**;12:505–515.
- [14] Smith AM, Mancini MC, Nie S. Bioimaging: second window for in vivo imaging. *Nat Nanotechnol.* **2009**;4:710–711.
- [15] So MK, Xu C, Andreas CX, et al. Self-illuminating quantum dot conjugates for *in vivo* imaging. *Nat Biotechnol.* **2006**;24:339–343.
- [16] Choi HS, Liu W, Misra P. Renal clearance of quantum dots. *Nat Biotechnol.* **2007**;25:1165–1170.
- [17] Wang R, Zhang F. NIR luminescent nanomaterials for biomedical imaging. *J Mater Chem B.* **2014**;2:2422–2443.
- [18] Hemmer E, Benayas A, Legare F, et al. Exploiting the biological windows: current perspectives on fluorescent bioprobes emitting above 1000 nm. *Nanoscale Horiz.* **2016**;1:168–184.
- [19] Zhao J, Zhong D, Zhou S. NIR-I-to-NIR-II fluorescent nanomaterials for biomedical imaging and cancer therapy. *J Mater Chem B.* **2018**;6:349–365.
- [20] Dubertret B, Skourides P, Norris DJ, et al. In vivo imaging of quantum dots encapsulated in phospholipid micelles. *Science.* **2002**;298:1759–1762.
- [21] Gao D, Zhang P, Sheng Z, et al. Highly bright and compact alloyed quantum rods with near infrared emitting: a potential multifunctional nanoplatfor for multimodal imaging in vivo. *Adv Funct Mater.* **2014**;24:3897–3905.
- [22] He Y, Zhong Y, Su Y, et al. Water-dispersed near-infrared-emitting quantum dots of ultra small sizes for in vitro and in vivo imaging. *Angew Chem Int Ed.* **2011**;50:5695–5698.
- [23] Geiregat P, Houtepen AJ, Sagar LK, et al. Continuous-wave infrared optical gain and amplified spontaneous emission at ultralow threshold by colloidal HgTe quantum dots. *Nat Mater.* **2018**;17:35–42.
- [24] Hu R, Yong KT, Roy I, et al. Functionalized near-infrared quantum dots for in vivo tumor vasculature imaging. *Nanotechnology.* **2010**;21:145105.
- [25] Qian H, Dong C, Peng J, et al. High-quality and water-soluble near-infrared photoluminescent CdHgTe/CdS quantum dots prepared by adjusting size and composition. *J Phys Chem C.* **2007**;111:16852–16857.
- [26] Liu X, Zhou P, Liu H, et al. Design of bright near-infrared-emitting quantum dots capped with different stabilizing ligands for tumor targeting. *RSC Adv.* **2018**;8:4221–4229.
- [27] Gao D, Zhang P, Jia J, et al. Ultra small paramagnetic near infrared quantum dots as dual modal nanoprob. *RSC Adv.* **2013**;3:21247–21250.
- [28] Yong KT, Roy I, Law WC, et al. Synthesis of cRGD-peptide conjugated near-infrared CdTe/ZnSe core-shell quantum dots for in vivo cancer targeting and imaging. *Chem Commun.* **2010**;46:7136–7138.
- [29] Hu D, Zhang P, Gong P, et al. A fast synthesis of near-infrared emitting CdTe/CdSe quantum dots with small hydrodynamic diameter for in vivo imaging probes. *Nanoscale.* **2011**;3:4724–4732.
- [30] Tao J, Zeng Q, Wang L. Near-infrared quantum dots based fluorescent assay of Cu²⁺ and in vitro cellular and in vivo imaging. *Sens Act B-Chem.* **2016**;234:641–647.
- [31] Lu Y, Su Y, Zhou Y, et al. In vivo behavior of near infrared-emitting quantum dots. *Biomaterials.* **2013**;34:4302–4308.
- [32] Semonin OE, Johnson JC, Luther JM, et al. Absolute photoluminescence quantum yields of IR-26 dye, PbS, and PbSe quantum dots. *J Phys Chem Lett.* **2010**;1:2445–2450.
- [33] Lignos I, Protesescu L, Stavrakis S, et al. Facile droplet-based microfluidic synthesis of monodisperse IV–VI semiconductor nanocrystals with coupled inline NIR fluorescence detection. *Chem Mater.* **2014**;26:2975–2982.
- [34] Du H, Chen C, Krishnan R, et al. Optical properties of colloidal PbSe nanocrystals. *Nano Lett.* **2002**;2:1321–1324.
- [35] Imamura Y, Yamada S, Tsuboi S, et al. Near-infrared emitting PbS quantum dots for in vivo fluorescence imaging of the thrombotic state in septic mouse brain. *Molecules.* **2016**;21:1080.
- [36] Yu Y, Zhang K, Sun S. One-pot aqueous synthesis of near infrared emitting PbS quantum dots. *Appl Surf Sci.* **2012**;258:7181–7187.
- [37] Tan TT, Selvan ST, Zhao L, et al. Size control, shape evolution, and silica coating of near-infrared-emitting PbSe quantum dots. *Chem Mater.* **2007**;19:3112–3117.
- [38] Zhao P, He K, Han Y, et al. Near-infrared dual-emission quantum dots–gold nanoclusters nanohybrid via co-template synthesis for ratiometric fluorescent detection and bioimaging of ascorbic acid in vitro and in vivo. *Anal Chem.* **2015**;87:9998–10005.
- [39] Benayas A, Ren F, Carrasco E, et al. PbS/CdS/ZnS Quantum dots: a multifunctional platform for in vivo near-infrared low-dose fluorescence imaging. *Adv Funct Mater.* **2015**;25:6650–6659.
- [40] Deng D, Zhang W, Chen X, et al. Facile synthesis of high-quality, water-soluble, near-infrared-emitting PbS quantum dots. *Eur J Inorg Chem.* **2009**;3440–3446.
- [41] Ma N, Marshall AF, Rao J. Near-infrared light emitting luciferase via biomineralization. *J Am Chem Soc.* **2010**;132:6884–6885.

- [42] Pietryga JM, Werder DJ, Williams DJ, et al. Utilizing the lability of lead selenide to produce heterostructured nanocrystals with bright, stable infrared emission. *J Am Chem Soc.* 2008;130:4879–4885.
- [43] Etgar L, Lifshitz E, Tannenbaum R. Hierarchical conjugate structure of γ -Fe₂O₃ nanoparticles and PbSe quantum dots for biological applications. *J Phys Chem C.* 2007;111:6238–6244.
- [44] Sasaki A, Tsukasaki Y, Komatsuzaki A, et al. Recombinant protein (EGFP-Protein G)-coated PbS quantum dots for in vitro and in vivo dual fluorescence (visible and second-NIR) imaging of breast tumors. *Nanoscale.* 2015;7:5115–5119.
- [45] Zamberlan F, Turyanska L, Patane A, et al. Stable DHLA-PEG capped PbS quantum dots: from synthesis to near-infrared biomedical imaging. *J Mater Chem B.* 2018;6:550–555.
- [46] Durmusoglu EG, Turke Y, Acar HY. Green synthesis of strongly luminescent, ultrasmall PbS and PbSe quantum dots. *J Phys Chem C.* 2017;121:12407–12415.
- [47] Gui R, Sun J, Liu D, et al. A facile cation exchange-based aqueous synthesis of highly stable and biocompatible Ag₂S quantum dots emitting in the second near-infrared biological window. *Dalton Trans.* 2014;43:16690–16697.
- [48] Tang H, Yang ST, Yang YF, et al. Blood clearance, distribution, transformation, excretion, and toxicity of near-infrared quantum dots Ag₂Se in mice. *ACS Appl Mater Interf.* 2016;8:17859–17869.
- [49] Javidi J, Haeri A, Hosseini F, et al. Synthesis, characterization, in vivo imaging, hemolysis, and toxicity of hydrophilic Ag₂S near-infrared quantum dots. *J Clust Sci.* 2017;28:165–178.
- [50] Song J, Ma C, Zhang W, et al. Bandgap and structure engineering via cation exchange: from binary Ag₂S to ternary AgInS₂, quaternary AgZnInS alloy and AgZnInS/ZnS core/shell fluorescent nanocrystals for bioimaging. *ACS Appl Mater Interf.* 2016;8:24826–24836.
- [51] Chen C, He X, Gao L, et al. Cation exchange-based facile aqueous synthesis of small, stable, and non-toxic near-infrared Ag₂Te/ZnS core/shell quantum dots emitting in the second biological window. *ACS Appl Mater Interf.* 2013;5:1149–1155.
- [52] Zhu CN, Jiang P, Zhang ZL, et al. Ag₂Se quantum dots with tunable emission in the second near-infrared window. *ACS Appl Mater Interface.* 2013;5:1186–1189.
- [53] Tan L, Wan A, Li H, et al. Conjugating S-nitrosothiols with glutathione stabilized silver sulfide quantum dots for controlled nitric oxide release and near-infrared fluorescence imaging. *ACS Appl Mater Interf.* 2013;5:11163–11171.
- [54] Tan L, Wan A, Zhao T, et al. Aqueous synthesis of multidentate-polymer-capping Ag₂Se quantum dots with bright photoluminescence tunable in a second near-infrared biological window. *ACS Appl Mater Interf.* 2014;6:6217–6222.
- [55] Tan L, Wan A, Li H. Synthesis of near-infrared quantum dots in cultured cancer cells. *ACS Appl Mater Interf.* 2014;6:18–23.
- [56] Ge XL, Zhang ZL, Xie ZX, et al. Revealing the biodistribution and clearance of Ag₂Se near-infrared quantum dots in mice. *New J Chem.* 2017;41:12721–12725.
- [57] Jiang P, Tian ZQ, Zhu CN, et al. Emission-tunable near infrared Ag₂S quantum dots. *Chem Mater.* 2012;24:3–5.
- [58] Dong B, Li C, Chen G, et al. Facile synthesis of highly photoluminescent Ag₂Se quantum dots as a new fluorescent probe in the second near-infrared window for in vivo imaging. *Chem Mater.* 2013;25:2503–2509.
- [59] Du Y, Xu B, Fu T, et al. Near-infrared photoluminescent Ag₂S quantum dots from a single source precursor. *J Am Chem Soc.* 2010;132:1470–1471.
- [60] Gu YP, Cui R, Zhang ZL, et al. Ultrasmall near-infrared Ag₂Se quantum dots with tunable fluorescence for in vivo imaging. *J Am Chem Soc.* 2012;134:79–82.
- [61] Zhang Y, Hong G, Zhang Y, et al. Ag₂S quantum dot: A bright and biocompatible fluorescent nanoprobe in the second near-infrared window. *ACS Nano.* 2012;6:3695–3702.
- [62] Zhang Y, Zhang Y, Hong G, et al. Biodistribution, pharmacokinetics and toxicology of Ag₂S near-infrared quantum dots in mice. *Biomaterials.* 2013;34:3639–3646.
- [63] Qin MY, Yang XQ, Wang K, et al. In vivo cancer targeting and fluorescence-CT dual-mode imaging with nanoprobe based on silver sulfide quantum dots and iodinated oil. *Nanoscale.* 2015;7:19484–19492.
- [64] Gui R, Wan A, Liu X, et al. Water-soluble multidentate polymers compactly coating Ag₂S quantum dots with minimized hydrodynamic size and bright emission tunable from red to second near-infrared region. *Nanoscale.* 2014;6:5467–5473.
- [65] Duman FD, Hocaoglu I, Ozturk DG, et al. Highly luminescent and cytocompatible cationic Ag₂S NIR-emitting quantum dots for optical imaging and gene transfection. *Nanoscale.* 2015;7:11352–11362.
- [66] Duman FD, Khodadust R, Durmusoglu EG, et al. Impact of reaction variables and PEI/L-cysteine ratio on the optical properties and cytocompatibility of cationic Ag₂S quantum dots as NIR bio-imaging probes. *RSC Adv.* 2016;6:77644–77654.
- [67] Shi LJ, Zhu CN, He H, et al. Near-infrared Ag₂Se quantum dots with distinct absorption features and high fluorescence quantum yields. *RSC Adv.* 2016;6:38183–38186.
- [68] Theodorou IG, Jawad ZAR, Qin H, et al. Significant metal enhanced fluorescence of Ag₂S quantum dots in the second near-infrared window. *Nanoscale.* 2016;8:12869–12873.
- [69] Zhang Y, Zhao N, Qin Y, et al. Affibody-functionalized Ag₂S quantum dots for photoacoustic imaging of epidermal growth factor receptor over-expressed tumors. *Nanoscale.* 2018;10:16581–16590.
- [70] Chen G, Tian F, Zhang Y, et al. Tracking of transplanted human mesenchymal stem cells in living mice using near-infrared Ag₂S quantum dots. *Adv Funct Mater.* 2014;24:2481–2488.
- [71] Chen G, Zhang Y, Li C, et al. Recent advances in tracking the transplanted stem cells using near-infrared fluorescent nanoprobe: turning from the first to the second near-infrared window. *Adv Healthc Mater.* 2018;7:1800497.
- [72] Torimoto T, Kameyama T, Kuwabata S, et al. Photo functional materials fabricated with chalcopyrite-type semiconductor nanoparticles composed of AgInS₂ and its solid solutions. *J Phys Chem Lett.* 2014;5:336–347.
- [73] Mao B, Chuang C, McCleese C, et al. Near-infrared emitting AgInS₂/ZnS nanocrystals. *J Phys Chem C.* 2014;118:13883–13889.

- [74] Xi Y, Yang J, Ge Y, et al. One-pot synthesis of water-soluble near-infrared fluorescence RNase A capped CuInS₂ quantum dots for in vivo imaging. *RSC Adv.* 2017;7:50949–50954.
- [75] Jiang T, Song J, Wang H, et al. Aqueous synthesis of color tunable Cu doped Zn–in–S/ZnS nanoparticles in the whole visible region for cellular imaging. *J Mater Chem B.* 2015;3:2402–2410.
- [76] Tan L, Liu S, Li X, et al. A new strategy for synthesizing AgInS₂ quantum dots emitting brightly in near-infrared window for in vivo imaging. *Coll Surf B Biointerf.* 2015;125:222–229.
- [77] Fahmi MZ, Chang JY. Potential application of oleylamine-encapsulated AgInS₂-ZnS quantum dots for cancer cell labeling. *Procedia Chem.* 2016;18:112–121.
- [78] Che D, Zhu X, Wang H, et al. Aqueous synthesis of high bright and tunable near-infrared AgInSe₂-ZnSe quantum dots for bioimaging. *J Coll Interf Sci.* 2016;463:1–7.
- [79] Liu S, Zhang H, Qiao Y, et al. One-pot synthesis of ternary CuInS₂ quantum dots with near-infrared fluorescence in aqueous solution. *RSC Adv.* 2012;2:819–825.
- [80] Qi K, Wang Y, Wang R, et al. Facile synthesis of homogeneous CuInS₂ quantum dots with tunable near-infrared emission. *J Mater Chem C.* 2016;4:1895–1899.
- [81] Xie R, Peng X. Synthesis of Cu-Doped InP Nanocrystals (d-dots) with ZnSe diffusion barrier as efficient and color-tunable NIR emitters. *J Am Chem Soc.* 2009;131:10645–10651.
- [82] Allen PM, Liu W, Chauhan VP. InAs (ZnCdS) quantum dots optimized for biological imaging in the near-infrared. *J Am Chem Soc.* 2010;132:470–471.
- [83] Liu Z, Kumbhar A, Xu D. Coreduction colloidal synthesis of III–V nanocrystals: the case of InP. *Angew Chem Int Ed.* 2008;120:3596–3598.
- [84] Bruns OT, Bischof TS, Harris DK, et al. Next-generation in vivo optical imaging with short-wave infrared quantum dots. *Nat Biomed Eng.* 2017;1:0056.
- [85] Gao J, Chen K, Xie R, et al. Ultrasmall near-infrared non-cadmium quantum dots for in vivo tumor imaging. *Small.* 2010;6:256–261.
- [86] Xu Q, Liu Y, Gao C, et al. Synthesis, mechanistic investigation, and application of photo luminescent sulfur and nitrogen co-doped carbon dots. *J Mater Chem C.* 2015;3:9885–9893.
- [87] Xu Q, Wan Y, Hu TS, et al. Robust self-cleaning and micromanipulation capabilities of gecko spatulae and their bio-mimics. *Nat Commun.* 2014;6:8949.
- [88] Xu Q, Xu H, Chen J, et al. Graphene and graphene oxide: advanced membranes for gas separation and water purification. *Inorg Chem Front.* 2015;2:417–424.
- [89] Xu Q, Zhao J, Liu Y, et al. Enhancing the luminescence of carbon dots by doping nitrogen element and its application in the detection of Fe (III). *J Mater Sci.* 2015;50:2571–2576.
- [90] Xu Q, Kuang T, Liu Y, et al. Hetero atom doped carbon dots: synthesis, characterization, properties, photoluminescence mechanism and biological applications. *J Mater Chem B.* 2016;4:7204–7219.
- [91] Ding H, Sb Y, Js W, et al. Full-color light emitting carbon dots with a surface-state-controlled luminescence mechanism. *ACS Nano.* 2015;10:484–491.
- [92] Zheng M, Li Y, Liu S, et al. One-pot to synthesize multifunctional carbon dots for near infrared fluorescence imaging and photo thermal cancer therapy. *ACS Appl Mater Interf.* 2016;8:23533–23541.
- [93] Pan L, Sun S, Zhang L, et al. Near-infrared emissive carbon dots for two-photon fluorescence bio imaging. *Nanoscale.* 2016;8:17350–17356.
- [94] Li L, Zhang R, Lu C, et al. In situ synthesis of NIR-light emitting carbon dots derived from spinach for bio-imaging applications. *J Mater Chem B.* 2017;5:7328–7334.
- [95] Lan M, Zhao S, Zhang Z, et al. Two-photon-excited near-infrared emissive carbon dots as multifunctional agents for fluorescence imaging and photothermal therapy. *Nano Res.* 2017;10:3113–3123.
- [96] Li D, Wang D, Zhao X, et al. Short-wave infrared emitted/excited fluorescence from carbon dots and preliminary applications in bioimaging. *Mater Chem Front.* 2018;2:1343–1350.
- [97] Li D, Jing P, Sun L, et al. Near-infrared excitation/emission and multiphoton-induced fluorescence of carbon dots. *Adv Mater.* 2018;30:1705913.
- [98] Carolan D. Recent advances in germanium nanocrystals: synthesis, optical properties and applications. *Prog Mater Sci.* 2017;90:128–158.
- [99] Shirahata N, Hirakawa D, Masuda Y, et al. Size-dependent color-tuning of efficiently luminescent germanium nanoparticles. *Langmuir.* 2013;29:7401–7410.
- [100] Ghosh B, Sakka Y, Shirahata N. Efficient green-luminescent germanium nanocrystals. *J Mater Chem A.* 2013;1:3747–3751.
- [101] Karatutlu A, Song M, Wheeler AP, et al. Synthesis and structure of free-standing germanium quantum dots and their application in live cell imaging. *RSC Adv.* 2015;5:20566–20573.
- [102] Lee DC, Pietryga JM, Rovel I, et al. Colloidal synthesis of infrared-emitting germanium nanocrystals. *J Am Chem Soc.* 2009;131:3436–3437.
- [103] Ghosh B, Ogawara M, Sakka Y, et al. Reductant-free colloidal synthesis of NIR emitting germanium nanocrystals: role of primary amine. *J Nanosci Nanotech.* 2014;14:2204–2210.
- [104] Ruddy DA, Johnson JC, Smith ER, et al. Size and bandgap control in the solution-phase synthesis of near-infrared-emitting germanium nanocrystals. *ACS Nano.* 2010;4:7459–7466.
- [105] Hessel CM, Reid D, Panthani MG, et al. Synthesis of ligand-stabilized silicon nanocrystals with size-dependent photoluminescence spanning visible to near-infrared wavelengths. *Chem Mater.* 2012;24:393–401.
- [106] Jurbergs D, Rogojjina D, Mangolini L, et al. Silicon nanocrystals with ensembles quantum yields exceeding 60%. *Appl Phys Lett.* 2006;88:233116.
- [107] Chandra S, Ghosh B, Beaune G, et al. Functional double-shelled silicon nanocrystals for two-photon fluorescence cell imaging: spectral evolution and tuning. *Nanoscale.* 2016;8:9009–9019.
- [108] Mastronardi ML, Laier-Flaig F, Faulkner D, et al. Size-dependent absolute photoluminescence quantum yields for size-separated colloidal-stable silicon nnaocrystals. *Nano Lett.* 2012;12:337–342.
- [109] Ghosh B, Takeguchi M, Nakamura J, et al. Origin of the photoluminescence quantum yields enhanced by alkane-termination of freestanding silicon nanocrystals: temperature-dependence of optical properties. *Sci Rep.* 2016;6:36951.

- [110] Ghosh B, Yamada H, Chinnathambi S, et al. Inverted device architecture for enhanced performance of flexible silicon quantum dot light-emitting diode. *J Phys Chem Lett.* **2018**;9:5400–5407.
- [111] Dohnalová K, Poddubny AN, Prokofiev AA, et al. Surface brightens up si quantum dots: direct bandgap-like size-tunable emission. *Lights Sci Appl.* **2013**;2:e47.
- [112] Priolo F, Gregorkiewicz T, Galli M, et al. Silicon nanostructures for photonics and photovoltaics. *Nat Nanotech.* **2014**;9:19–32.
- [113] Liu X, Zhao S, Gu W, et al. Light-emitting diodes based on colloidal silicon quantum dots with octyl and phenylpropyl ligands. *ACS Appl Mater Interf.* **2018**;10:5959–5966.
- [114] Ghosh B, Hamaoka T, Nemoto Y, et al. Impact of anchoring monolayers on the enhancement of radiative recombination in light emitting diodes based on silicon nanocrystals. *J Phys Chem C.* **2018**;122:6422–6430.
- [115] Chinnathambi S, Chen S, Ganesan S, et al. Silicon quantum dots for biological applications. *Adv Healthc Mater.* **2014**;3:10–29.
- [116] Chinnathambi S, Chen S, Ganesan S, et al. Binding mode of CpG oligodeoxynucleotides to nanoparticles regulates bifurcated cytokine induction via toll-like receptor 9. *Sci Rep.* **2012**;2:534.
- [117] Chinnathambi S, Pi X, Xu M, et al. Regulation of bifurcated cytokine induction by surface charge of nanoparticles during interaction between CpG oligodeoxynucleotides and toll-like receptor 9. *J Drug Deliv Sci Technol.* **2015**;29:251–260.
- [118] Mazzaro R, Romano F, Ceroni P. Long-lived luminescence of silicon nanocrystals: from principles to applications. *Phys Chem Chem Phys.* **2017**;19:26507–26526.
- [119] Ghosh B, Shirahata N. Colloidal silicon quantum dots: synthesis and luminescence tuning from the near-UV to the near-IR range. *Sci Technol Adv Mater.* **2014**;15:014207.
- [120] Su Y, Ji X, He Y. Water-dispersible fluorescent silicon nanoparticles and their optical applications. *Adv Mater.* **2016**;28:10567–10574.
- [121] Dohnalová K, Gregorkiewicz T, Kúsová K. Silicon quantum dots: surface matters. *J Phys Cond Matter.* **2014**;26:173201.
- [122] Dasog M, Kehrle J, Rieger B, et al. Silicon nanocrystals and silicon-polymer hybrids: synthesis, surface engineering, and applications. *Angew Chem Int Ed.* **2015**;54:2–20.
- [123] Shirahata N. Colloidal Si nanocrystals: A controlled organic-inorganic interface and its implications of color-tuning and chemical design toward sophisticated architectures. *Phys Chem Chem Phys.* **2011**;13:7284–7294.
- [124] Bfp M, Tilley RD. Solution synthesis, optical properties, and bioimaging applications of silicon nanocrystals. *Acc Chem Res.* **2014**;47:3045–3051.
- [125] Wheeler LM, Neale NR, Chen T, et al. Hypervalent surface interactions for colloidal stability and doping of silicon nanocrystals. *Nat Commun.* **2013**;4:2197.
- [126] Kelly JA, Veinot JGC. An investigation into near-UV hydrosilylation of freestanding silicon nanocrystals. *ACS Nano.* **2010**;4:4645–4656.
- [127] Chandra S, Masuda Y, Shirahata N, et al. transition-metal-doped NIR-emitting silicon nanocrystals. *Angew Chem Int Ed.* **2017**;56:6157–6160.
- [128] Henderson EJ, Kelly JA, Veinot JGC. Influence of HSiO_{1.5} sol-gel polymer structure and composition on the size and luminescence properties of silicon nanocrystals. *Chem Mater.* **2009**;21:5426–5434.
- [129] Yu Y, Fan G, Fermi A, et al. Size-dependent photoluminescence efficiency of silicon quantum dot. *J Phys Chem C.* **2017**;121:23240–23248.
- [130] Ghosh B, Masuda Y, Wakayama Y, et al. Hybrid white light emitting diode based on silicon nanocrystals. *Adv Funct Mater.* **2014**;24:7151–7160.
- [131] Sun W, Qian C, Mastronardi ML, et al. Hydrosilylation kinetics of silicon nanocrystals. *Chem Commun.* **2013**;49:11361–11363.
- [132] Hori Y, Kano S, Sugimoto H, et al. Size-dependence of acceptor and donor levels of boron and phosphorus codoped colloidal silicon nanocrystals. *Nano Lett.* **2016**;16:2615–2620.
- [133] Ni Z, Pi X, Zhou S, et al. Size-dependent structures and optical absorption of boron-hyperdoped silicon nanocrystals. *Adv Opt Mater.* **2016**;4:700–707.
- [134] Sugimoto H, Fujii M, Fukuda Y, et al. All-inorganic water-dispersible silicon quantum dots: highly efficient near-infrared luminescence in a wide pH range. *Nanoscale.* **2014**;6:122–126.
- [135] Wang L, Reipa V, Blasic J. Silicon nanoparticles as a luminescent label to DNA. *Bioconj Chem.* **2004**;15:409–412.
- [136] Yong KT, Law WC, Hu R, et al. Nanotoxicity assessment of quantum dots: from cellular to primate studies. *Chem Soc Rev.* **2013**;42:1236.
- [137] Ruizendaal L, Bhattacharjee S, Pournazari K, et al. Synthesis and cytotoxicity of silicon nanoparticles with covalently attached organic monolayers. *Nanotoxicology.* **2009**;3:339–347.
- [138] Alshgarif NH, Berger CEM, Varanasi SS, et al. Alkyl-capped silicon nanocrystals lack cytotoxicity and have enhanced intercellular accumulation in the malignant cells via cholesterol-dependent endocytosis. *Small.* **2009**;19:221–228.
- [139] He GS, Zheng Q, Yong KT. Two- and three-photon absorption and frequency upconverted emission of silicon quantum dots. *Nano Lett.* **2008**;8:2688–2692.
- [140] Ravotto L, Chen Q, Ma Y, et al. Bright long-lived luminescence of silicon nanocrystals sensitized by two-photon absorbing antenna. *Chem.* **2017**;2:550–560.
- [141] Sakiyama M, Sugimoto H, Fujii M. Long-lived luminescence of colloidal silicon quantum dots for time-gated fluorescence imaging in the second near infrared window in biological tissue. *Nanoscale.* **2018**;10:13902–13907.
- [142] Wang H-C, Bao Z, Tsai H-Y, et al. Perovskite quantum dots and their application in light-emitting diodes. *Small.* **2018**;14:1702433.
- [143] Noh YW, Kong SH, Choi DY, et al. Near-infrared emitting polymer nanogels for efficient sentinel lymph node mapping. *ACS Nano.* **2012**;6:7820–7831.
- [144] Hameed S, Chen H, Irfan M, et al. Fluorescence guided sentinel lymph node mapping: from current molecular probes to future multimodal nanoprobe. *Bioconjugate Chem.* **2019**;30:13–28.
- [145] Kim S, Lim YT, Soltész EG, et al. Near-infrared fluorescent type II quantum dots for sentinel lymph node mapping. *Nat Biotechnol.* **2004**;22:93–97.
- [146] Robe A, Pic E, Lassalle HP, et al. Quantum dots in axillary lymph node mapping: biodistribution study in healthy mice. *BMC Cancer.* **2008**;22:111.
- [147] Wu Q, Chu M. Self-illuminating quantum dots for highly sensitive in vivo real-time luminescent mapping

- of sentinel lymph nodes. *Int J Nanomedicine*. [2012](#);7:3433–3443.
- [148] Si C, Zhang Y, Lv X, et al. In vivo lymph node mapping by Cadmium Tellurium quantum dots in rats. *J Surg Res*. [2014](#);192:305–311.
- [149] Pons T, Pic E, Lequeux N, et al. Cadmium-free CuInS₂/ZnS quantum dots for sentinel lymph node imaging with reduced toxicity. *ACS Nano*. [2010](#);4:2531–2538.
- [150] Erogbogbo F, Yong KT, Roy I, et al. In vivo targeted cancer imaging, sentinel lymph node mapping and multi-channel imaging with biocompatible silicon nanocrystals. *ACS Nano*. [2011](#);5:413–423.